

¹ A robust method for measuring ² aminoacylation through tRNA-Seq

³ Kristian Davidsen^{1,2} and Lucas B Sullivan^{1*}

*For correspondence:
lucas@fredhutch.org (LBS)

⁴ ¹Fred Hutchinson Cancer Center; ²Molecular and cellular biology program, University of
⁵ Washington

⁶

⁷ **Abstract** tRNA aminoacylation levels are difficult to quantify with current methods having either
⁸ low throughput or low precision and/or accuracy. We present an optimized charge tRNA-Seq
⁹ method combining new and previously described developments to generate precise and accurate
¹⁰ tRNA charge measurements. We show several controls and tests for validation of quantitation and
¹¹ provide an end-to-end method that scales to hundreds of samples including software for data
¹² processing. Our method also supports using the charge tRNA-Seq data to determine relative
¹³ expression levels and reverse transcription misincorporations to infer RNA modifications.

¹⁴

¹⁵ Introduction

¹⁶ Quantification of transfer RNA (tRNA) aminoacylation, also referred to as charge, has been per-
¹⁷ formed using radiolabeling (*Wolfson and Uhlenbeck, 2002*), Northern blotting (*Ho and Kan, 1987*;
¹⁸ *Varshney et al., 1991; Stenum et al., 2017*), DNA microarrays (*Dittmar et al., 2005*) and high-
¹⁹ throughput sequencing (*Evans et al., 2017*). While radiolabeling is highly accurate, it is limited
²⁰ to purified tRNAs undergoing lab manipulation. Northern blotting uses differential migration of
²¹ acylated tRNA during electrophoresis to measure acylation levels but has many known limitations
²² such as cross-binding probes, low sensitivity, low throughput on multiple tRNAs, insufficient band
²³ separation etc. Chemical differentiation of acylated tRNAs combined with DNA microarrays were
²⁴ introduced to circumvent the problems with Northern blotting, but has since been superseded by
²⁵ high-throughput sequencing approaches that enable quantification on all tRNAs in one experiment.

²⁶ Chemical differentiation of acylated tRNAs is achieved using the Malaprade reaction to attack
²⁷ the 2,3-dihydroxyls on the 3' ribose of deacylated tRNA, causing ring opening and destabilization.
²⁸ The destabilized base is then eliminated using high pH and heat, resulting in a one base truncated
²⁹ 3' sequence of uncharged tRNAs compared to those protected by aminoacylation. This sequence
³⁰ of reactions was characterized and used extensively in the past in an effort to sequence RNA
³¹ molecules (*Whitfeld and Markham, 1953; Whitfeld, 1954; Khy and Cohn, 1961; Neu and Heppel,*
³² *1964*), and while futile for RNA sequencing, the single base truncation has proven highly useful
³³ to "tag" deacylated tRNAs. We shall refer to this reaction sequence as the "Whitfeld reaction"
³⁴ (*Figure 1—figure Supplement 1*).

³⁵ The accuracy and robustness of aminoacylation measurements depend on two parts: the
³⁶ completeness of the Whitfeld reaction and the quality of tRNA sequencing (tRNA-Seq). A major
³⁷ problem in tRNA-Seq is base modifications known to be numerous on tRNAs. These can lead
³⁸ to stalling, misincorporation, skipping or falloff during the reverse transcription (RT) step of the
³⁹ sequencing protocol (*Motorin et al., 2007*). The RT polymerase is most severely affected by base
⁴⁰ modifications disrupting the Watson–Crick base pairing, while other modifications are often less
⁴¹ impactful or silent (*Wang et al., 2021; Sas-Chen and Schwartz, 2019*). To increase RT readthrough
⁴² the demethylase AlkB has been used (*Zheng et al., 2015; Cozen et al., 2015*), while more recently

43 optimization of incubation conditions, including low salt and extended incubation time, can similarly
44 increase readthrough (*Behrens et al., 2021*). Several other factors can also lead to errors in tRNA-Seq
45 such as low RNA integrity, incomplete deacylation prior to adapter ligation, adapter ligation bias,
46 PCR amplification bias and errors in read alignment, necessitating further protocol optimization to
47 overcome these issues.

48 Adapter ligation bias is another well documented problem in small RNA sequencing (*Fuchs
49 et al., 2015; Zhuang et al., 2012*), but receives little attention in most tRNA-Seq protocols where it is
50 particularly problematic because adapters often incorporate a barcode for sample multiplexing.
51 The problem is further exacerbated when tRNA-Seq is coupled with the Whitfeld reaction, because
52 this creates different sequence contexts for ligation of aminoacylated and deacylated tRNAs. One
53 solution is to optimize conditions such that the ligation goes to completion. To that end, the tRNA
54 secondary structure provides a useful opportunity as it contains four nucleotides on the 3' end
55 that do not participate in the basepairing of the acceptor stem. These are the discriminator base
56 followed by the invariant CCA-end (*Figure 1*). These free nucleotides can be engaged in basepairing
57 by an oligo splint designed to guide the ligation of the adapter and can improve tRNA specificity
58 and ligation efficiency (*Shigematsu et al., 2017; Smith et al., 2015*).

59 Read mapping is another known problem for tRNA-Seq. It arises due to the high error-rate
60 of the RT polymerase when reading through modified bases in addition to frequent falloff. In
61 combination, reads will often not have any continuous stretch of more than 15 nt. that perfectly
62 match its reference. This is a problem for almost all alignment algorithms because they rely on
63 some variation of subsequence matching to enable speed-up. The problem has been addressed by
64 clustering of the reference sequences (*Hoffmann et al., 2018*) as well as masking known modified
65 positions in the reference sequences (*Behrens et al., 2021*).

66 In recent years many variations of the tRNA-Seq method have been published (*Wang et al.,
67 2021; Zheng et al., 2015; Cozen et al., 2015; Shigematsu et al., 2017; Erber et al., 2020; Thomas
68 et al., 2021; Lucas et al., 2023; Pinkard et al., 2020; Warren et al., 2021; Yamagami and Hori, 2022*),
69 but only few couple it with the Whitfeld reaction to probe aminoacylation levels (*Evans et al., 2017;
70 Behrens et al., 2021; Watkins et al., 2022*) and little is known about the precision and accuracy of
71 these measurements. Here, we present an up-to-date method for charge tRNA-Seq that integrates
72 new and existing developments, including improved Whitfeld reaction chemistry, splint assisted
73 ligation, high readthrough RT-PCR and improved read mapping, enabling us to measure tRNA
74 charge, expression and modifications (*Figure 1*). We perform tests of the quantitative capabilities of
75 the method and determine its precision and accuracy. Finally, we provide an open-source code
76 repository, enabling others to use our read processing, mapping and statistical tools on their own
77 data (<https://github.com/krdav/tRNA-charge-seq>).

78 Results

79 Optimizing the Whitfeld reaction for charge tRNA-Seq

80 The use of periodate oxidation to discriminate aminoacylated tRNA by sequencing was first used by
81 *Dittmar et al. (2005)* for microarray measurements and then elegantly adapted to high-throughput
82 sequencing by *Evans et al. (2017)*. However, we found noticeable differences between the conditions
83 reported optimal for periodate oxidation in biochemical assays in the past (*Khym and Cohn, 1961;
84 Neu and Heppel, 1964; Khym and Uziel, 1968; Dyer, 1956*) and those used in charge tRNA-Seq today
85 (*Evans et al., 2017; Behrens et al., 2021; Watkins et al., 2022; Pavlova et al., 2020; Tsukamoto et al.,
86 2022*). We therefore reasoned that it would be valuable to find a set of optimal conditions for the
87 Whitfeld reaction when applied to charge tRNA-Seq. To do this, we used an E.coli tRNA-Lys-CCA
88 oligo and measured conversion to its 1 nt. truncated product.

89 Periodate oxidation of cis-glycols is known to occur rapidly, even at low temperature (*Dyer,
90 1956*); therefore, we tested if oxidation could be performed on ice to protect tRNA aminoacylations
91 prone to hydrolysis. We found that complete oxidation is achieved after just 5 min (*Figure 2*, panel

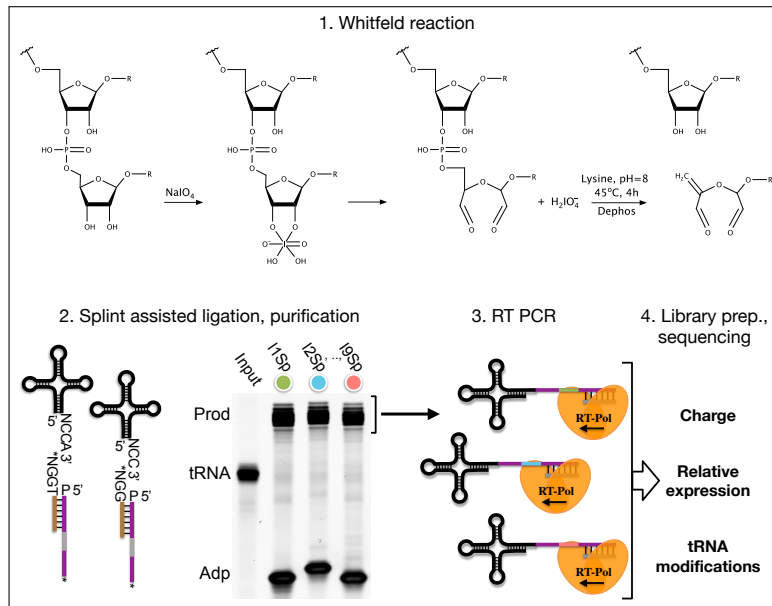


Figure 1. Summary illustrating the steps of the charge tRNA-Seq method we used to measure aminoacylation, relative expression and tRNA modification levels. First, the Whitfeld reaction (detailed in *Figure 1—figure Supplement 1*) is used to discriminate between tRNAs with and without an aminoacylation by cleaving off the 3' base of deacylated tRNA. Second, the tRNA secondary structure exposes the discriminator base (N) followed by the CCA/CC-end, creating a sticky-end for splint assisted ligation to a barcoded adapter. Stars (*) on the 3' end of splint and adapter oligos indicate modifications to block self-ligation. Third, using the purified ligation product, RT-PCR is used to generate cDNA. Fourth, the cDNA is converted into a dsDNA library and sequenced to determine tRNA charge, expression and modifications.

Figure 1—figure supplement 1. Whitfeld reaction scheme.

92 A) and therefore chose 10 min as optimal, with incubation on ice and in the dark because sunlight
93 induces periodate oxidation side-reactions (*Erskine et al., 1953*).

94 Oxidation of deacylated tRNA yields a dialdehyde on the terminal ribose which enables the
95 phosphoric ester linkage to be broken in a β -elimination reaction (*Rammler, 1971; Uziel, 1973*),
96 yielding an unsaturated product (*Figure 1—figure Supplement 1*). While this cleavage reaction is
97 complex, involving several semi-stable intermediates and different pathways depending on the pH,
98 it appears to be induced by high pH and the presence of a primary amine (*Uziel, 1975*). Lysine has
99 been identified as a good source of primary amine and incubation at 45°C has been found optimal
100 (*Khym and Cohn, 1961; Neu and Heppel, 1964*). In previous charge tRNA-Seq methods, a borax
101 buffered solution at pH=9.5 has been used to induce cleavage, instead we wanted to test using lysine
102 at pH=8 to improve RNA stability. We found complete cleavage after just 10 min (*Figure 2*, panel B);
103 however, this step also serves as deacylation step and some aminoacylations were still measurable
104 after up to 90 min of lysine cleavage (*Figure 2—figure Supplement 1*, panel A). Therefore, we settled
105 on a 4 h incubation time, but even with this extended incubation, the decrease in pH made a large
106 improvement on RNA integrity (*Figure 2*, panel C).

107 Finally, we wanted to perform the Whitfeld reaction as a one-pot reaction as shown by *Watkins*
108 *et al. (2022)*. However, we found that the typical quenchers used to remove unreacted periodate (glucose or ribose) are not compatible with lysine induced cleavage (*Figure 2—figure Supplement 1*, panel C). This is likely due to the generation of dialdehydes that cross-link lysines; therefore, we chose to use ethylene glycol which forms formaldehyde upon periodate quenching. Additionally, ethylene glycol reacts fast and can be added in high molar excess without negatively affecting subsequent steps, thus enabling the whole Whitfeld reaction in one tube (*Figure 2*, panel D).

114 **Blunt-end adapter ligation introduces charge measurement bias**
115 Following the Whitfeld reaction tRNAs must be sequenced in order to measure aminoacylation
116 levels. To achieve this with enough throughout, we chose to ligate the samples to barcoded adapters
117 to enable sample pooling before the RT-PCR step (*McGlincy and Ingolia, 2017*). We followed the
118 protocol of *Behrens et al. (2021)*, with minor modifications to the oligo design, but found that the
119 measured charge was highly variable between replicates and that the measurements were biased by
120 the barcode identity to an unacceptable degree (*Figure 2—figure Supplement 2*). We hypothesized
121 that this is due to ligation bias commonly encountered in blunt-end ligation (*Fuchs et al., 2015;*
122 *Zhuang et al., 2012; Jayaprakash et al., 2011*) and reasoned that increasing ligation efficiency could
123 mitigate the bias. However, our attempts to improved ligation efficiency failed as we were never
124 able to reach more than ~50% ligation of the input tRNA (*Figure 2—figure Supplement 3*).

125 **Splint assisted ligation improves efficiency**

126 Inspired by *Smith et al. (2015)* and *Shigematsu et al. (2017)* we turned to splint assisted ligation.
127 This approach utilizes that tRNAs have four nucleotides protruding from the 3' end and therefore
128 available for basepairing: the discriminator base, which can be any of the four RNA nucleotides,
129 followed by the invariant CCA-end. The splint oligo is designed to bind both the 3' end of tRNAs
130 and the 5' end of an adapter (*Figure 1*), thus bringing the two into proximity and increasing ligation
131 efficiency. However, whereas earlier uses of splint assisted ligation could assume that all tRNAs
132 end on CCA, we have a mix of CCA and CC-ending tRNAs and therefore needed to use two splints.
133 As tRNAs compete for ligation it is imperative that CCA-ending tRNAs, with stronger interaction with
134 the splint, is not favoured over CC-ending tRNAs. Fortunately, we observed a near complete ligation
135 between all of our nine barcoded adapters and both CCA-ending human tRNA and a CC-ending
136 E. Coli tRNA-Lys oligo (*Figure 2—figure Supplement 4*, panel A and B). The ligation was specific
137 as it was fully dependent on complementarity between the tRNA and the splint (*Figure 2—figure*
138 *Supplement 4*, panel C). As we are only interested in ligation between tRNA and adapter, we block all
139 other possible ligations through dephosphorylation of the 5' tRNA nucleotide and oligo modifications
140 blocking the 3' end of adapter and splint oligos. This affords us the advantage of using a pure
141 DNA splint without any RNA nucleotides as those used in previous publications (*Smith et al., 2015;*
142 *Shigematsu et al., 2017; Pinkard et al., 2020; Warren et al., 2021; Thomas et al., 2021; Lucas et al.,*
143 *2023*).

144 Importantly, we validated that tRNA processed using the one-pot Whitfeld reaction could be
145 effectively used as substrate in the ligation reaction (*Figure 2*, panel E and *Figure 2—figure Supple-*
146 *ment 5*, panel A). We noted that a small amount of unligated tRNA appeared in reactions with tRNA
147 oxidized with periodate. This unligated tRNA is of unknown origin and largely refractory to further
148 ligation (*Figure 2—figure Supplement 5*, panel B); however, as shown later using charge titration,
149 this did not have a measurable impact on the accuracy of the aminoacylation measurement.

150 **Combining optimizations results in a robust method for measuring tRNA charge**

151 After combining the optimized Whitfeld reaction with subsequent splint assisted ligation, we used
152 the RT-PCR method proposed by *Behrens et al. (2021)* using the TGIRT polymerase (*Mohr et al.,*
153 *2013*) to maximize the readthrough of modified nucleotides. We later found that almost as high
154 readthrough could be achieved using Maxima RT polymerase (*Figure 2—figure Supplement 6*). The
155 RT-PCR was primed by an oligo containing a 10 nt. unique molecular identifier (UMI) to diversify
156 the sequence context for the subsequent circular ligation and allow collapsing of reads derived
157 from the same tRNA molecule during data analysis. A final PCR was performed to attach Illumina
158 barcodes to pool samples for multiplex sequencing.

159 Using this as our final charge tRNA-Seq method, we use the E.coli tRNA-Lys-CCA oligo as a
160 spike-in control before the Whitfeld reaction to validate near complete conversion to its CC-end
161 product, suggesting efficient periodate oxidation (*Figure 2—figure Supplement 7*, panel A). Similarly,
162 we validated the completeness of deacylation using deacylated controls and the integrity of the

163 tRNA CCA-end using non-oxidized controls (*Figure 2—figure Supplement 7*, panel B and C). We
164 then measured the baseline charge of H1299 cells grown in DMEM using four replicates, observing
165 excellent repeatability and high charge for most codons except tRNA^{Ser} codons and a tRNA^{Glu} codon,
166 validating observation by *Evans et al. (2017)* (*Figure 2*, panel F).

167 Reference masking improves read mapping

168 It has previously been noted that alignment of tRNA reads is challenging due to RT misincorporations
169 and falloff (*Hoffmann et al., 2018; Behrens et al., 2021*). Most commonly, the Bowtie1 or Bowtie2
170 aligners have been applied using various settings to accommodate short reads and the many
171 mismatches (*Cozen et al., 2015; Zheng et al., 2015; Clark et al., 2016; Evans et al., 2017; Pinkard*
172 *et al., 2020*). However, while these are ultra-fast and widely used for RNA-Seq, Bowtie1 does not support alignments with insertions or deletions, and although Bowtie2 does, it does not guarantee that the best alignment is returned (*Langmead et al., 2009; Langmead and Salzberg, 2012*). We reasoned that many users of tRNA-Seq would rather sacrifice computational speed than mapping accuracy and therefore we apply a full all-against-all local alignment using the Smith-Waterman algorithm to provide the guaranteed best alignment(s). This is possible because the set of tRNA transcripts in a typical species is only a few hundred sequences and thus we are able to align 1e8 tRNA-Seq reads to a human tRNA reference with 457 sequences in less than 8 h on an Intel Core i7-8700K Processor (12 threads, 4.70 GHz).

181 In addition to the choice of read alignment method, *Behrens et al. (2021)* found that using
182 a SNP-tolerant alignment substantially improved mapping when modified positions causing RT
183 misincorporations were defined as SNPs. We adapted this approach by masking modified positions
184 in the reference to "N"; however, we cannot rely solely on annotated modifications because these
185 are incomplete and their effect on RT misincorporation rates is hard to predict. Instead, we used
186 the misincorporation information embedded in the sequencing data, extracting it after a first
187 pass alignment and then using mismatch frequencies to pick positions for reference masking. As
188 such, this is an iterative process because the alignment will change slightly with a new masked
189 reference. In addition to the number of iterations, masking is only applied on positions with
190 a minimum mismatch frequency (`min_mut_freq`) and frequency is calculated either including
191 or excluding reads with multiple transcript alignments (`unique_anno_float`). Furthermore, a
192 parameter (`frac_max_score`) controls the sharing of a mask to highly similar transcripts. To find
193 the optimal combination of parameters for reference masking we performed a grid search with the
194 objective of finding the masking that resulted in the least number of reads assigned to transcripts
195 with multiple codons (*Figure 3*, panel A). This lead to 533 positions in the 455 sequence reference
196 getting masked and resulting in an alignment improvement, reducing the reads with multiple codon
197 alignments from 11.71% to 5.09%.

198 Masked positions do not contribute to the alignment score and thus possibly lowering it below
199 the minimum threshold; however, we observed no trade-off between optimized reference masking
200 and read mapping percentage (*Figure 3*, panel B). Like *Behrens et al. (2021)*, we observe a striking
201 difference in the mapping of certain tRNA transcripts with inosine at the first position of the
202 anticodon (position 34; I34). For example, transcripts decoding the Ser-UCU codon (IGA anticodon)
203 (*Figure 3*, panel C). Generally, reference masking appears to increase annotations for around a
204 dozen transcripts but a substantial mapping change only occurs for six codons (*Figure 3—figure*
205 *Supplement 1*, panel a). The effect of reference masking on the charge measurements was low as
206 expected because this is a relative number (*Figure 3—figure Supplement 1*, panel B).

207 tRNA modifications are reflected in mismatches, gaps and RT stops
208 Our computational method also supports using misincorporation data for inference of nucleotide
209 modifications, which is typically only valid for modifications that disrupt Watson-Crick base pairing
210 such as methylations (*Clark et al., 2016; Behrens et al., 2021*). As such the 5-methoxycarbonylmethyl-
211 2-thiouridine (mcm5s2U) modification should be silent; however, thionucleosides are sensitive to

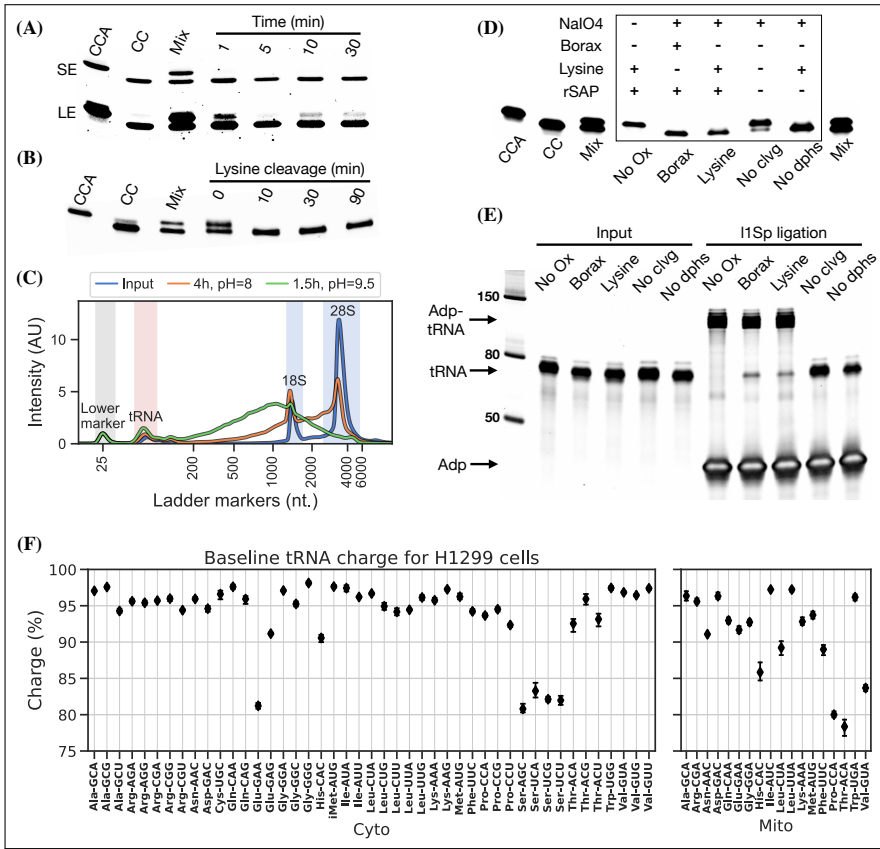


Figure 2. Optimizing the chemistry of charge tRNA-Seq. **(A)** Time required to complete periodate oxidation of the E.coli tRNA-Lys-CCA oligo on ice. Following oxidation, RNA was processed similar to [Evans et al. \(2017\)](#) to cleave off the 3' adenosine. Successful cleavage produce E.coli tRNA-Lys-CC. CCA, input oligo. CC, product oligo. Mix, 50/50 mix of CCA and CC. SE, short exposure. LE, long exposure. **(B)** Time required to complete lysine cleavage of the E.coli tRNA-Lys-CCA oligo (CCA) at 45°C, pH=8. Cleavage at time 0 is likely due to the heat denaturation step performed in RNA loading buffer prior to running the gel. **(C)** TapeStation electropherogram comparing stability of whole cell RNA before and after 4 h lysine cleavage at pH=8 or 1.5 h borax cleavage at pH=9.5. tRNA range marked by red background, 18/28S by blue. See [Figure 2—figure Supplement 1](#), panel B for RNA stability timecourse as it occurs on a gel. **(D)** Effect of individual components on cleavage of the E.coli tRNA-Lys-CCA oligo (CCA). All samples were processed as a one-pot reaction, except the borax sample which was processed similar to [Evans et al. \(2017\)](#). rSAP, shrimp alkaline phosphatase. **(E)** Ligation test comparing the effect of RNA processing. Deacylated and gel purified human tRNA was processed identically as in panel (D), then ligated to adapter l1Sp. Other adapters were tested with similar results ([Figure 2—figure Supplement 5](#), panel A). **(F)** Baseline tRNA aminoacylation charge in H1299 cells grown in DMEM (4 replicates, bootstrapped 95% confidence interval of the mean). Charge on tRNA^{His} is possibly erroneously low because the discriminator base is shielded by base pairing ([Heinemann et al., 2012](#)), creating a steric hindrance for the splint assisted ligation.

Figure 2—figure supplement 1. Optimizing lysine induced cleavage.

Figure 2—figure supplement 2. Measurement bias in charge tRNA-Seq using blunt-end ligation.

Figure 2—figure supplement 3. tRNA-adapter blunt-end ligation attempted optimization.

Figure 2—figure supplement 4. Splint assisted ligation is highly efficient.

Figure 2—figure supplement 5. Ligation tests, related to panel E.

Figure 2—figure supplement 6. RT readthrough comparing TGIRT to Maxima.

Figure 2—figure supplement 7. Sequenced controls.

Figure 2—figure supplement 8. tRNA homology requires careful PCR conditions.

212 periodate treatment, which oxidizes them to sulfonates and makes them sensitive to nucleophilic
213 attack ([Ziff and Fresco, 1968; Rao and Cherayil, 1974](#)). When periodate oxidation of mcm5s2U is

followed by lysine cleavage it would presumably result in a lysine adduct (*Ziff and Fresco, 1968*), thus disrupting Watson–Crick base pairing. We verified this by comparing the misincorporation signature in samples processed with/without periodate oxidation, focusing on the human tRNAs Lys-UUU, Gln-UUG, Glu-UUC and Arg-UCU shown by *Lentini et al. (2018)* to carry the mcm5s2U modification (**Figure 3—figure Supplement 2**). Large changes in the misincorporation signature is observed upon periodate oxidation, but curiously some tRNAs respond with a large decrease in RT readthrough while others have an increased mutation and/or gap frequency. Similar observations were recently showed by *Katanski et al. (2022)*.

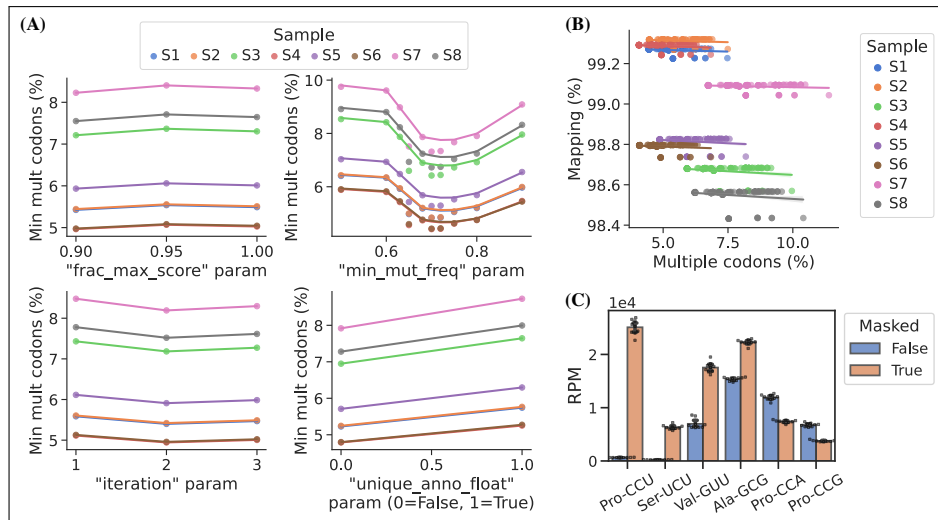


Figure 3. Masking of the reference sequences improves alignment performance. **(A)** Grid search optimization of parameters determining the extent of reference masking (see method section for details). Each subplot shows the mean effect of one tuning parameter when combined with the combination of all the other three. Parameters used for reference masking are chosen to minimize the percentage of reads assigned to tRNAs with multiple codons. **(B)** There is no trade-off between sequence mapping success and minimizing multiple codon mapping. **(C)** Reference masking increase relative expression levels of select codons. Reads per million (RPM) levels of the codons shown was found before and after optimized reference masking. Error bars are bootstrapped 95% confidence interval of the mean over the 9 barcode replicate samples.

Figure 3—figure supplement 1. Reference masking effect on RPM and charge levels.

Figure 3—figure supplement 2. Anticodon modification mcm5s2U is detected in periodate oxidized samples.

Barcode replicates show high precision

To assess measurement precision, we performed our charge tRNA-Seq protocol on the same tRNA sample using all nine barcoded adapters. We used partially deacylated RNA to achieve a representative spread of aminoacylation levels within a single sample (*Figure 4—figure Supplement 2*, panel A) and then extracted differences compared to the median barcode replicate measurement. When comparing charge measurements binned by barcode, we observed that most were narrowly distributed with the median close to zero indicating little or no barcode bias (*Figure 4*, panel A). Adapter I4Sp is the exception that proves why barcode bias needs to be investigated, because it is consistently overestimating charge levels, with a median overestimate of ~3 percentage points. Overall however, charge measurements show high precision with a standard deviation from the median of just 1.7 percentage points, with similar results at the transcript level (*Figure 4—figure Supplement 1*, panel A).

For RPM values, some barcode replicates were more narrowly distributed than others. However, these differences are small and with a standard deviation from the median of 5.1 percentage we consider the RPM measurements to be precise (*Figure 4*, panel B and *Figure 4—figure Supplement 1*, panel B).

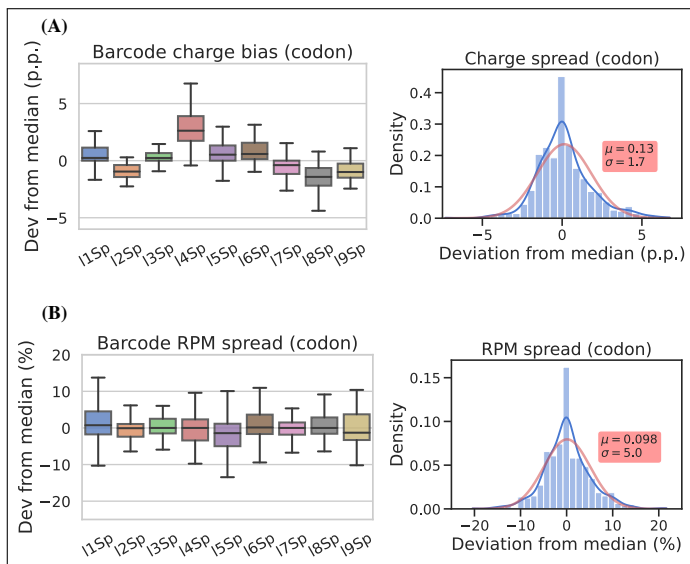


Figure 4. Barcode replicates show high precision and limited barcode bias. Each of the nine adapters were ligated to the same sample containing a heterogeneous mix of CC and CCA-ending tRNAs. Ligations were then pooled and submitted to the remainder of the charge tRNA-Seq protocol. **(A)** The percentage point deviation from the median charge at the codon level, grouped by barcode identity (left) or shown summarized as a density plot (right). **(B)** The percentage deviation from the median RPM at the codon level, grouped by barcode identity (left) or shown summarized as a density plot (right). Density plots are provided with kernel density estimate (KDE) in blue, normal distribution estimate in red and inserts with mean (μ) and standard deviation (σ). For plots of transcript level data see *Figure 4—figure Supplement 1*.

Figure 4—figure supplement 1. Charge and RPM deviation at the transcript level.

Figure 4—figure supplement 2. Best and worst barcode replicates.

238 Charge titration shows high accuracy

239 Testing the accuracy of charge measurements is a much harder problem. Spiking in a defined ratio
 240 of CC and CCA-ending oligo to the ligation reaction is a common approach, but this ignores the
 241 possible incompleteness of the Whitfeld reaction. It is also possible to compare to charge measured
 242 by Northern blotting, but this presents a different set of issues with probe annealing, band resolution
 243 etc. As an alternative, we made a charge titration by mixing different proportions of intact and
 244 deacylated RNA allowing us to predict and measure charge levels of over 150 transcripts (*Figure 5*,
 245 panel A). The results showed excellent proportionality between predicted and measured charge
 246 across the full range of values (*Figure 5*, panel B), thus indicating that the charge measurements
 247 are highly accurate. This experiment also confirmed our previous observations that barcode
 248 bias is limited to the 14Sp adapter, which is consistently overestimating charge (*Figure 5*, panel
 249 C). Additionally, no bias was found in independently prepared sequencing libraries or any of the
 250 different mixing proportions of intact and deacylated RNA (*Figure 5—figure Supplement 2*).

251 Inspired by *Evans et al. (2017)*, which used radiolabeling techniques to generate a single accurate
 252 tRNA charge reference point, we developed a 50% charge control using 3' phosphorylation as
 253 protection from periodate oxidation. This control was spiked into samples before the Whitfeld
 254 reaction and showed a mean charge of 50.36% and a standard deviation of 1.11 percentage points
 255 (*Figure 5—figure Supplement 3*, panel B), thus further validating the measurement accuracy of our
 256 method.

257 Charge tRNA-Seq enables measurement of aminoacylation half-lives of native tRNAs

258 tRNA aminoacylations are prone to hydrolysis and the effect of pH and temperature on their decay
 259 rates has previously been studied (*Hentzen et al., 1972*). Interestingly, *Peacock et al. (2014)* found
 260 that the aminoacylation half-life appeared to be determined solely by the identity of the amino acid

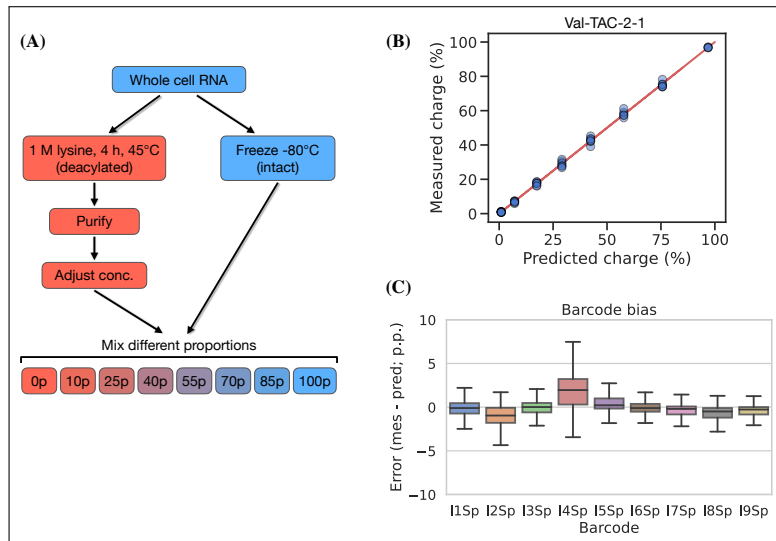


Figure 5. Charge titration shows linearity over the full range of charge measurements. **(A)** Schematic illustration of the method to generate samples with predictable charge percentages. **(B)** Titration data for a representative tRNA transcript, Val-TAC-2-1, with the red line indicating proportionality between predicted and measured charge. For reference, the best and worst fitting tRNA transcripts are shown in *Figure 5—figure Supplement 1*. **(C)** Error binned by adapter barcode. Error is the percentage point difference between the measured vs. predicted charge for all transcripts in the bin.

Figure 5—figure supplement 1. Best and worst fitting transcripts for charge titration.

Figure 5—figure supplement 2. Error binned by sequencing run and titration sample.

Figure 5—figure supplement 3. Spike-in control for 50% charge.

attachment and not affected significantly by the tRNA sequence or RNA modifications. However, most of the tRNAs used in this study were derived from in vitro transcription and only a limited set of RNA modifications were tested; additionally, the study did not cover all 20 native amino acids. Having developed an accurate method for measuring tRNA charge on over a hundred samples in a single sequencing run, we wanted to use this to determine the aminoacylation half-lives of tRNA transcripts with their native RNA modifications.

We used RNA purified from the H1299 cell line, starting at high tRNA charge (*Figure 2*, panel F), and tracked the aminoacylation decay over time after switching to physiological buffer (pH=7.2) and incubating at 20°C, similar to *Peacock et al. (2014)*. After sampling 11 timepoints with 4 replicates, charge measurements for each transcript were fitted to a first-order decay function to estimate the half-life of each transcripts (Supplementary file 4), as exemplified by the representative transcript Lys-TTT-3-1 (*Figure 6*, panel A). When transcripts were grouped by their cognate amino acid, we could confirm that the half-lives are indeed determined mostly by aminoacylation identity and that they span a 37 fold range (*Figure 6*, panel B). Our half-life estimates are highly correlated with those reported by *Peacock et al. (2014)*, but surprisingly ours appear to be approximately 4 fold higher despite using the same incubation temperature and a similar buffer, with only slightly lower pH (7.2 vs. 7.5; *Figure 6—figure Supplement 1*, panel B).

It seems counterintuitive that the aminoacylation half-life should be completely unaffected by the tRNA sequence; however, as the amino acid is attached to the invariant CCA-end, the nucleotides most proximal to the ester bond are the same for all tRNAs. The most proximal non-invariant nucleotide is the discriminator base. Because we sample all transcripts, we are able to observe that the discriminator base is indeed likely to influence the half-life and that a purine base appears to promote a longer aminoacylation half-life than a uracil (*Figure 6*, panel C).

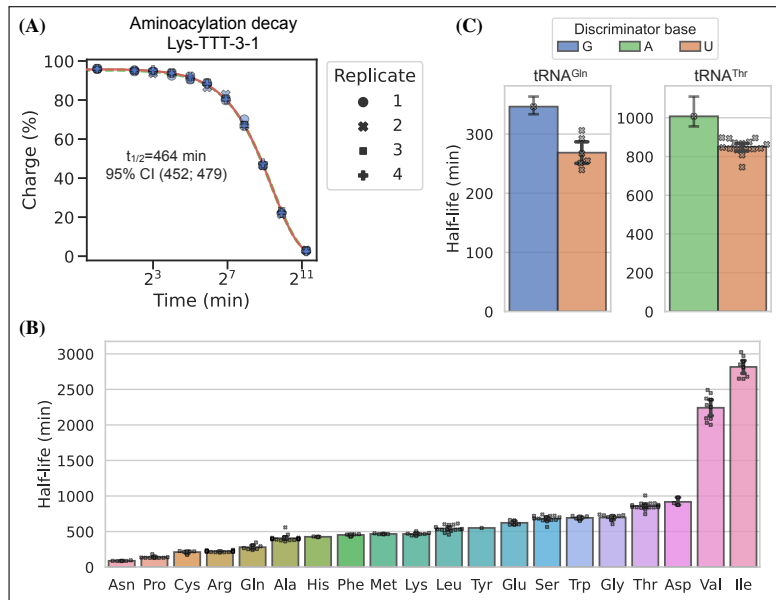


Figure 6. Measuring aminoacylation half-life using charge tRNA-Seq. **(A)** Aminoacylation decay for a representative tRNA transcript Lys-TTT-3-1 over the 11 timepoints sampled. For reference, the best and worst fitting tRNA transcripts are shown in *Figure 6—figure Supplement 2*. The fitted first-order decay to estimate the aminoacylation half-life is shown as a red line. Similar dashed lines are plotted in green for the bootstrapped 95% confidence interval (these are hard to see). **(B)** Aminoacylation half-life estimates grouped by amino acid. Each marker represents one transcript, errorbars are bootstrapped 95% confidence intervals of the mean. **(C)** Distribution of aminoacylation half-life estimates for tRNA^{Gln} and tRNA^{Thr} transcripts grouped by discriminator base identity. Errorbars are bootstrapped 95% confidence intervals. For the single transcripts with G or A discriminator base the bootstrap is performed on measurement replicates while for the U discriminator base it is performed on the transcript observations.

Figure 6—figure supplement 1. RNA integrity and comparison to previous half-life values.

Figure 6—figure supplement 2. Best and worst transcript half-life estimates.

284 Discussion

285 Accurate quantification is a prerequisite for making reliable observations standing the test of time
 286 and replication. We have presented a robust method for measuring tRNA charge and extensively
 287 validated it in the relevant context of human tRNA. Furthermore, we have quantified the mea-
 288 surement precision of charge and relative expression. Accuracy was only quantified for charge
 289 measurement whereas this is more challenging for expression levels (*Fuchs et al., 2015*). One step
 290 towards accurate expression level measurements is efficient adapter ligation, such as the splint
 291 assisted ligation method used herein; however, future versions of tRNA-Seq should strive towards
 292 providing better validation and controls for relative expression measurements. In our version of
 293 the Whitfeld reaction we use lysine to induce base cleavage at low pH. We later found that ornithine
 294 is an even better inducer of cleavage (*Uziel, 1975*) and thus, the pH of the cleavage reaction could
 295 be lowered even further and possibly combined with Cu⁺² as a deacylation catalyst (*Kroll, 1952;*
Schofield and Zamecnik, 1968) to shorten incubation times.

297 In our experience, as well as others (*Shigematsu et al., 2017*), splint assisted ligation is highly
 298 efficient compared to blunt-end ligation. In contrast, *Behrens et al. (2021)* achieved high efficiency
 299 blunt-end ligation, allowing inclusion of non-mature tRNAs without the normal CCA-end. While
 300 the reason for this discrepancy is not obvious, our results highlight the difficulty of using blunt-
 301 end ligations for tRNA-Seq and provide an alternative approach of splint assisted ligation to help
 302 mitigate those issues. One potential issue with our approach is that the tRNA^{His} sequence is not
 303 ideal for splint assisted ligation due to the additional G added to the 5' end (*Heinemann et al., 2012*)
 304 and thus shielding the discriminator base from base pairing with the splint. Despite this, reads

305 mapping to tRNA^{His} are surprisingly abundant and both CC and CCA-ending. In future versions
306 of this method, we see the possibility of combining our optimizations with the on-bead sample
307 processing developed by *Watkins et al. (2022)* to eliminate gel purification steps and achieve faster
308 and cleaner processing.

309 We solve the tRNA alignment problem by non-heuristic alignment which is guaranteed to return
310 the best alignment. This is computationally demanding but nevertheless quite possible on the small
311 number of tRNA transcript references. A more challenging problem is the application of reference
312 masking to improve the annotation accuracy. We used unique codon annotation as the objective in
313 our optimization, but this is a surrogate as the ground truth in unknown. Further improvements
314 could be achieved by simulation of tRNA reads including realistic RT misincorporations, indels
315 and falloff and optimizing alignment to this simulated ground truth. Additionally, annotation
316 performance could be increased further using tools, such as a as hidden Markov models (HMMs),
317 to model complex phenomena such as interaction between modifications (*Wang et al., 2021*;
318 *Hernandez-Alias et al., 2022*).

319 In summary, we report a robust charge tRNA-Seq method that has been thoroughly tested and
320 validated as precise and accurate for charge measurements.

321 Methods and Materials

322 Cell culture and RNA extraction

323 The human cell line H1299 was acquired from ATCC and tested to be free from mycoplasma
324 (Mycoprobe, R&D Systems). Cells were maintained in Dulbecco's Modified Eagle's Medium (DMEM)
325 supplemented with 3.7 g/L sodium bicarbonate, 10% fetal bovine serum (FBS) and 1% penicillin-
326 streptomycin solution. Cells were incubated in a humidified incubator at 37°C with 5% CO₂.

327 For RNA extraction, cells were seeded onto a 15 cm dish and grown in DMEM until confluence.
328 The cells were then removed from the incubator, placed on a slope on ice and media was quickly
329 and thoroughly aspirated before adding 3 mL Trizol to cover all the cells. From this point onward,
330 everything was kept ice cold to prevent hydrolysis of the aminoacylation. After a 2 mins incubation,
331 the cell material was scraped down the slope mixing it with the Trizol, then 2x1.5 mL was transferred
332 to 2 mL Eppendorf tubes and 0.3 mL chloroform was added. The tubes were vortexed 2 min and
333 then centrifuged (17,000g, 5 mins). From each tube, 0.75 mL of the upper layer was transferred to
334 a tube with 0.8 mL isopropanol (IPA), then mixed and incubated 60 mins at -20°C. Tubes were then
335 centrifuged (17,000g, 15 mins) and RNA pellets were washed twice with 1 mL 80% IPA containing 100
336 mM sodium acetate (pH=4.5). These washing steps are critical because Trizol contains glycerol which
337 will react with and inhibit the subsequent periodate oxidation step. A last wash was performed
338 using 1 mL 100% IPA and after removing the supernatant the RNA pellets were air-dried at room
339 temperature, then stored dry at -80°C.

340 Charge tRNA-Seq using blunt-end ligation

341 For charge tRNA-Seq using blunt-end ligation shown in *Figure 2—figure Supplement 2* the protocol
342 described by *Behrens et al. (2021)* was followed with the exception of using different adapter
343 sequences, a UMI containing RT oligo (Supplementary file 1), more rounds of amplification and
344 gel based size selection for the final sequence library and using paired-end sequencing. Briefly,
345 whole cell RNA was extracted, reconstituted in 100 mM sodium acetate (pH=4.5) and concentration
346 adjusted to 1 µg/µL. A 20 µL sample was move to a new tube and submitted to periodate oxidation
347 and 3' base elimination using sodium borate as described by *Evans et al. (2017)*. After purification
348 and reconstitution in water, 8 ng of a 50/50 mix of E.coli tRNA-Lys-CCA and E.coli tRNA-Lys-CC oligo
349 was added as a CCA/CC ratio control. The true ratio of these oligos is hard to control because each
350 contain a different fraction of truncated oligos that will not contribute to the number of mapped
351 reads; however, the sequenced CCA/CC ratio is an important measure of the sample to sample
352 variance. Then the RNA was 3' dephosphorylated using T4 PNK and after another round of RNA

353 purification the tRNA fraction was isolated on a 10% Urea-TBE gel using SYBRGold staining and
354 a blue light transilluminator for visualization. After gel elution and reconstitution in water, 100
355 ng tRNA was transferred to a PCR tube and ligated to 20 pmol pre-adenylated adapter (I1, I2, I3
356 or I4) in 25% PEG-8000, 1xT4 RNA ligase buffer using 1 μ L T4 RNA ligase 2 (truncated KQ) and 1
357 μ L Superaseln. Prior to ligation adapters were adenylated using the NEB 5' DNA Adenylation Kit
358 following the manufacturers instruction. After purification, adapter adenylation was verified using
359 differential gel migration. Ligation reactions were incubated 6 h at 25°C, pooled by adapter barcode
360 and purified, followed by isolation of the ligation product from unligated tRNA using a 10% Urea-TBE
361 gel.

362 After gel elution and reconstitution in water, the RT-PCR reaction was performed as described
363 by *Behrens et al. (2021)* using a similar RT oligo but with an extra 9 random nucleotides at the
364 5'-end to act as a unique molecular identifier (UMI). After the RT-PCR incubation, the remainder of
365 the sample processing follows the charge tRNA-Seq sample processing described below, including
366 cDNA circularization, Illumina P7/P5 sequence attachment and sequencing.

367 Charge tRNA-Seq method optimization

368 Optimization of the oxidation, cleavage and dephosphorylation, collectively called the Whitfeld
369 reaction (*Whitfeld and Markham, 1953*), was done using oligos E.coli tRNA-Lys-UUU-CCA and E.coli
370 tRNA-Lys-UUU-CC (Supplementary file 1; anticodon omitted from name below). Both oligos were gel
371 purified on a 10% Urea-TBE gel to resolve full length from truncated oligos. First, the time required
372 for oxidation was tested, following the same quenching and borax buffered high pH induced
373 cleavage used by *Evans et al. (2017)*. For this, samples of 35 ng E.coli tRNA-Lys-CCA were prepared
374 in 10 μ L 100 mM sodium acetate (pH=4.5) and used as substrate for the Whitfeld reaction conversion
375 to E.coli tRNA-Lys-CC. Reaction progress was monitored on a 10% Urea-TBE gel by resolving the
376 one nucleotide difference using the substrate, the product and a 50/50 mix as markers. Also using
377 this approach, we tested using lysine induced cleavage (*Khym and Cohn, 1961*) by swapping the
378 sodium borate used for cleavage with 1 M lysine (pH=8). The cleavage step also includes deacylation
379 and to verify the completeness of this, four samples of 10 μ g whole cell RNA were prepared in
380 10 μ L 100 mM sodium acetate (pH=4.5) and incubated with 50 μ L 1 M lysine (pH=8) at 45°C for
381 5, 30, 90 and 270 min. Then, 1 mL ice cold 80% isopropanol containing 100 mM sodium acetate
382 (pH=4.5) was added, RNA was precipitated, washed twice, dried and reconstituted in 10 μ L 100 mM
383 sodium acetate (pH=4.5). These deacylated samples were then submitted to the charge tRNA-Seq
384 sample processing described below, except using lysine at pH=9.5 and 90 min incubation at 45°C to
385 ensure complete deacylation. From this, incubation time in lysine (pH=8) was chosen to be 4 h. To
386 compare the RNA integrity after cleavage with lysine vs. borax, samples of 10 μ g whole cell RNA
387 were prepared in 10 μ L 100 mM sodium acetate (pH=4.5) and added 50 μ L of either 1 M lysine (pH=8)
388 or 100 mM sodium borate (pH=9.5). Tubes were incubated 45°C and samples taken at time 0, 1.5, 4
389 and 8 h. RNA integrity was determined using TapeStation (high sensitivity RNA) and 10% Urea-TBE
390 gel. Upon combining the steps of the Whitfeld reaction to a one-pot reaction a color change was
391 observed after addition of lysine. To test the effect of the periodate quencher, 10 μ L of freshly
392 prepared 200 mM NaIO4 in 100 mM sodium acetate (pH=4.5) was quenched by 10 μ L 1 M aqueous
393 solution of either ethylene glycol (*Neu and Heppel, 1964*), glycerol (*Alefelder et al., 1998*), glucose
394 (*Evans et al., 2017*), ribose (*Watkins et al., 2022*) or water (control) for 10 min at room temperature.
395 Then 100 μ L 1 M lysine at either pH 8 or 9.5 was added and reactions incubated at 45°C for 4 h
396 before moving to room temperature for visual inspection (*Figure 2—figure Supplement 1*, panel C).

397 For ligation optimization human tRNA was isolated from H1299 cells. First, whole cell RNA was
398 isolated as described above, reconstituted in water and deacylation at 45°C in 1 M lysine (pH=8) for
399 4 h. Then RNA was purified using the Monarch RNA Cleanup Kit (50 μ g) and run on a 10% Urea-TBE
400 gel to resolve the tRNA from mRNA and rRNA. tRNA was defined as the range between 70 and 85
401 nt. as approximated by the low range ssRNA ladder. For blunt-end ligations in *Figure 2—figure*
402 *Supplement 3*, 40 ng tRNA, either isolated from H1299 cells or as E.coli tRNA-Lys-CC oligo, was

403 ligated to 20 pmol pre-adenylated adapter in a 20 μ L reaction containing 25% PEG-8000, 200 U T4
404 RNA ligase 2 (truncated KQ; RnI2tr KQ), 10 U SUPERaseln and the vendor provided buffer. For splint
405 assisted ligation in *Figure 2—figure Supplement 4*, 35 ng tRNA, either isolated from H1299 cells or as
406 E.coli tRNA-Lys-CC oligo, was ligated to 20 pmol annealed adapter:splint partial duplex as described
407 for charge tRNA-Seq sample processing below. For the non-complementary splint test, two splint
408 oligos were made with CAAC and AAC overhangs (Supplementary file 1) and annealed to adapter
409 I1Sp. For the ligation test in *Figure 2*, panel E and *Figure 2—figure Supplement 5*, panel A, 500 ng
410 tRNA isolated from H1299 cells was subjected to the one-pot Whitfeld reaction described for charge
411 tRNA-Seq sample processing below but with a single step removed. For the no oxidation sample
412 NaIO4 was replaced with NaCl, for the no dephosphorylation sample shrimp alkaline phosphatase
413 (rSAP) was replaced with water and for the no cleavage sample RNA was purified after periodate
414 quenching. These were compared to a sample processed as described in *Evans et al. (2017)*. All
415 samples were purified using the Monarch RNA Cleanup Kit and 35 ng was used per ligation test
416 with adapters I1Sp, I2Sp and I3Sp using the ligation protocol described for charge tRNA-Seq sample
417 processing below.

418 **Charge tRNA-Seq sample processing**

419 Stepwise description with details in Supplementary file 2. Whole cell RNA was reconstituted in
420 100 mM sodium acetate (pH=4.5) and keep on ice until the end of the periodate oxidation step.
421 For deacylated control samples, RNA was prepared by first performing a deacetylation step on the
422 input RNA by incubation in 1 M lysine (pH=8) at 45°C for 4 h, followed by purification using the
423 Monarch RNA Cleanup Kit (50 μ g). The RNA concentration was adjusted to 1 μ g/ μ L, 10 μ L was
424 transferred to a fresh tube and 1 μ L E.coli tRNA spike-in control was added. Initially, the spike-in
425 control contained 5 ng/ μ L E.coli tRNA-Lys-CCA, later 5 ng/ μ L of each E.coli tRNA-Thr-CGT CCA-Phos
426 and E.coli tRNA-Thr-CGT CCA was also included. To this 5 μ L freshly prepared 200 mM NaIO4 was
427 added following 10 min incubation on ice, in the dark. For non-oxidized control samples, NaCl
428 was used instead of NaIO4. The oxidation was quenched by adding 5 μ L 50% (v/v) ethylene glycol
429 (~9 M) and incubating for 5 min on ice and 5 min at room temperature, in the dark. Then 50 μ L
430 1 M lysine (pH=8) with 1 μ L Superaseln was added and tubes were incubate for 4 h at 45°C. To
431 dephosphorylate RNA 8 μ L 10X rCutSmart Buffer and 1 μ L rSAP was added followed by 30 min
432 incubation at 37°C. RNA was then purified using the Monarch RNA Cleanup Kit (50 μ g), eluting with
433 30 μ L water. A 6 μ L sample was then denatured by mixing with 2x urea loading buffer (8 M urea, 30
434 mM sodium acetate, 2 mM EDTA, 0.02 % (w/v) bromophenol blue and xylene cyanol, pH adjusted to
435 4.7-5) and incubating 2 min at 90°C. The tRNA fraction was then isolated on a 10% Urea-TBE gel
436 using SYBRGold staining and a blue light transilluminator for visualization. Gel elution was done by
437 crushing the gel with a disposable pestle, adding 200 μ L gel elution buffer and 1 μ L Superaseln, then
438 snap freezing in liquid nitrogen and incubating at 65°C for 5 mins with shaking. This gel slurry was
439 filtered through a Spin-X filter followed by tRNA purification using the Oligo Clean & Concentrator kit.
440 The concentration of purified tRNA was measured, then it was annealed in NEBuffer 2 by heating to
441 94°C for 2 min followed by cooling 1°C/s to 4°C. 35 ng of the annealed tRNA was transferred to a
442 PCR tube and to this was added 20 pmol annealed adapter:splint partial duplex, 1 μ L 10x NEBuffer
443 2, 2 μ L 10x T4 RNA ligase buffer, 4 μ L 50% PEG-8000, 1 μ L Superaseln and 1 μ L T4 RNA ligase 2. The
444 annealed adapter:splint partial duplex was made by making an equimolar mix of the CCA and CC
445 splint oligos, then using this to make an equimolar mix with the adapter oligo and annealing this in
446 NEBuffer 2 by heating to 94°C for 2 min followed by cooling 0.3°C/s to 4°C. Each ligation reaction
447 was adjusted to 20 μ L with water, mixed and incubated 1 h at 37°C followed by 24 h at 4°C and heat
448 inactivation at 80°C for 5 min. Samples were pooled by adapter barcode, purified using the Oligo
449 Clean & Concentrator kit and then ligated tRNA was isolated on a gel and purified similarly to the
450 initial tRNA isolation.

451 Reverse transcription was setup with 60 ng of the purified adapter ligated tRNA as template
452 using the buffer composition, incubation temperature and time suggested by *Behrens et al. (2021)*.

453 To 10 μ L template in a PCR tube, 2 μ L 1.25 μ M RT oligo and 4 μ L RT buffer was added following
454 denaturation and annealing by incubation at 90°C for 2 min, 70°C for 30 s and cooling 0.2°C/s to
455 4°C. Then, to each tube 1 μ L 100 mM DTT, 1 μ L Superaseln and 1 μ L TGIRT-III RT polymerase (or
456 Maxima H Minus for *Figure 2—figure Supplement 6*) was added following 10 min incubation at
457 42°C. Then 1 μ L 25 mM dNTPs was added and the incubation was resumed at 42°C for 16 h on a
458 thermocycler with the heated lid set to 50°C. The RNA template was hydrolyzed by adding 1 μ L 5 M
459 NaOH followed by incubation at 95°C for 3 min. The samples were then purified using the Oligo
460 Clean & Concentrator kit and the cDNA was isolated on a gel and purified similarly to the initial
461 tRNA isolation, eluting with 7 μ L water. cDNA was circularized by transferring 5.5 μ L cDNA to a PCR
462 tube and adding 2 μ L 5 M betaine, 1 μ L 10x CircLigase buffer, 0.5 μ L 1 mM ATP, 0.5 μ L 50 mM MnCl₂
463 and 0.5 μ L CircLigase. The reaction was incubated at 60°C for 3 h on a thermocycler with a 70°C
464 heated lid, then the enzyme was deactivated by denaturing at 80°C for 10 min.

465 PCR was used to attach Illumina P7/P5 sequences to flank the tRNA insert. Each PCR reaction
466 was setup to contain 0.6 μ L circularized cDNA, 1.5 μ L 10 mM dNTPs, 5 μ L 10 μ M P7 oligo, 5 μ L 10
467 μ M P5 oligo, 10 μ L 5x KAPA HiFi buffer, 1 μ L KAPA HiFi polymerase and 26.9 μ L water. The PCR
468 reactions were incubated at 95°C for 3 min followed by 3 cycles of 98°C for 20 s, 68°C for 10 s
469 and 72°C for 15 s, and then followed by X cycles of 98°C for 20 s and 72°C for 15 s, with X being
470 empirically determined (*Figure 2—figure Supplement 8*, panel A). The optimal number of PCR cycles
471 were determined by preparing three PCR reactions, incubating them with X=10, 12 and 14 and
472 running 4 μ L of each reaction on a 4-12% TBE gel. The PCR reactions with optimal X, resulting
473 in abundant amplification product with little PCR crossover, were purified using the DNA Clean
474 & Concentrator-5 kit and resolved on a 4-12% TBE gel. The gel was stained using SYBRGold and
475 visualized using a blue light transilluminator to isolated the library DNA by cutting out the size range
476 covering all possible insert lengths (170-290 bp). Gel elution was done by crushing the gel with
477 a disposable pestle, adding 300 μ L TBE, snap freezing in liquid nitrogen and incubating at room
478 temperature overnight with mixing. If necessary, elution time could be decreased by incubation
479 at higher temperature; although, this required adding higher salt concentrations to prevent DNA
480 reannealing (*Figure 2—figure Supplement 8*, panel B). The gel slurry was filtered through a Spin-X
481 filter following DNA purification using the DNA Clean & Concentrator-5 kit and eluting with 20 μ L
482 10 mM Tris (pH=8). DNA with different Illumina P7/P5 barcodes were pooled for multiplexing and
483 sequenced using Illumina paired end sequencing using 2x100 bp reads.

484 E.coli tRNA spike-in control

485 An E.coli tRNA spike-in control was generated from oligos E.coli tRNA-Lys-UUU-CCA and E.coli
486 tRNA-Thr-CGT-CCAA (anticodon sometimes omitted from name). First, 2 μ g per well of the E.coli
487 tRNA-Lys-CCA oligo was loaded on a 10% Urea-TBE gel to resolve full length from truncated oligos.
488 After gel elution and purification using the Oligo Clean & Concentrator kit the RNA concentration
489 was measured and adjusted such that 5 ng was spiked into each sample of 10 μ g whole cell RNA
490 before periodate oxidation. Adding the control before periodate oxidation afforded an internal
491 control of the completeness of the oxidation reaction.

492 Second, 30 μ L of 100 μ M E.coli tRNA-Thr-CCAA oligo was submitted to a partial Whitfeld reaction,
493 stopping before the dephosphorylation step. The oxidation reaction was performed by adding 10
494 μ L 100 mM sodium acetate (pH=4.5) and 20 μ L 200 mM NaIO₄ followed by incubation for 30 min
495 at room temperature in the dark. Oxidation was quenched using 20 μ L 50% ethylene glycol and
496 incubated 30 min at room temperature in the dark. Then buffer exchange was performed using a P-6
497 gel column pre-equilibrated with 100 mM lysine (pH=8). To the eluate 400 μ L 1 M lysine (pH=8) and
498 1 μ L Superaseln was added followed by 5 h incubation at 45°C and purification using the Monarch
499 RNA Cleanup Kit (using two 50 μ g columns). The product, a 1 nt. truncated and 3' phosphorylated
500 oligo named E.coli tRNA-Thr-CCA-Phos, was resolved on a gel to isolate the full length oligo, as
501 described for the other control. Half of this product was submitted to dephosphorylation using
502 rSAP and purified using the Oligo Clean & Concentrator kit yielding E.coli tRNA-Thr-CCA. Complete

503 phosphorylation of E.coli tRNA-Thr-CCA-Phos and complete dephosphorylation of E.coli tRNA-Thr-
504 CCA was verified using ligation (*Figure 5—figure Supplement 3*, panel A). Then concentrations of
505 both E.coli tRNA-Thr-CCA-Phos and E.coli tRNA-Thr-CCA was measured to generate an equimolar
506 mix adjusted such that 10 ng was spiked into each sample of 10 µg whole cell RNA before periodate
507 oxidation. The 3' phosphorylation protects from periodate oxidation and thus adding it before
508 periodate oxidation afforded an internal control of a 50% charged tRNA, probing the completeness
509 of the whole Whitfeld reaction and potential adapter ligation bias.

510 **Oligo design**

511 For adapters used for blunt-end ligation the design was similar to *McGlincy and Ingolia (2017)* and
512 *Behrens et al. (2021)*, with a 5' phosphorylation to enable adenylation and a 3' dideoxycytidine to
513 prevent self-ligation and concatemer formation. For adapters I1, I2, I3 and I4 the barcode sequence
514 was 8 nt. starting at the 5', for adapters I1N, I2N and I3N the barcode sequence was truncated
515 to 5 nt. to make space for a preceding six random nucleotides to diversify the sequence context
516 engaged in ligation.

517 The design of adapters used for splint assisted ligation was influenced by *Smith et al. (2015)*
518 and *Shigematsu et al. (2017)* but with several important differences listed below. First, we do
519 not use ribonucleotides at any positions in our adapters or splint oligos. This affords us higher
520 quality oligos due to the higher coupling efficiency of deoxyribose during oligo synthesis as well as
521 robustness against hydrolysis of DNA compared to RNA. A primary reason to use ribonucleotides in
522 the adapters and splint oligos is to increase ligation efficiency; however, we achieved ~100% ligation
523 efficiency on isolated human tRNA using our design without ribonucleotides (*Figure 2—figure*
524 *Supplement 4*, panel A). Second, instead of ligating the adapter to the 3' and the splint to the 5'
525 of the tRNA, we only ligate the adapter and block the splint from ligating using a 3' C3 spacer,
526 as well as dephosphorylating the 5' of the tRNA. Similar to the blunt-end ligation adapters, a 3'
527 dideoxycytidine is included on all adapters to block self-ligation and concatemer formation. Third,
528 we use two different lengths splint oligos with overhang compatible with NCCA and NCC-ending
529 tRNA. Fourth, our adapters vary in length by the size of their barcodes, from 5 to 8 nt. This is to
530 offset the sequencing reading frame of read P2 (P7) as it progresses into the 3' end of the tRNA,
531 thus increasing the sequence diversity and base calling quality.

532 The RT-PCR oligo was designed in a similar way as *McGlincy and Ingolia (2017)* and *Behrens*
533 *et al. (2021)* with a 5' phosphorylation for subsequent circular ligation of the cDNA and an 18-atom
534 hexa-ethyleneglycol spacer (iSp18) to terminate the polymerase extension and avoiding rolling-
535 circle amplification during the PCR to attach Illumina P7/P5 sequences. The RT oligo has a random
536 purine base on the 5' to increase circular ligation efficiency. We added an additional 9 random
537 nucleotides following this purine to increase the diversity of the sequence engaged in circular
538 ligation. These random nucleotides also provide a unique molecular identifier (UMI) with 524288
539 possible sequences that enable collapsing of reads derived from the same tRNA molecule. The
540 UMI is also used as a general sample quality control by comparing the number of observed UMI
541 sequences with the number expected. The expected number unique UMI observations is calculated
542 as:

$$E[X] = n \left[1 - \left(\frac{n-1}{n} \right)^k \right] \quad (1)$$

543 With $E[X]$ being the expected number of unique UMI observations, n being the number of reads
544 for the particular sample and k being the number of possible UMIs.

545 The final dsDNA library was designed as an Illumina TruSeq dual index library with combined i5
546 and i7 indices attached by PCR with P7/P5 oligos. These oligos were synthesized with a phosphoroth-
547 ioate bond between the last two nucleotides to prevent degradation by the KAPA HiFi polymerase.
548 An overview of the RNA/DNA manipulations including ligation of adapters, RT-PCR, circularization
549 and library PCR is provided in Supplementary file 3.

550 **Read processing**

551 Reads were first demultiplexed according to their i7/i5 barcodes. Read pairs were then trimmed
552 and merged using AdapterRemoval:

```
553 AdapterRemoval --preserve5p --collapse --minalignmentlength 10 --adapter1  
554     AGATCGGAAGAGCACACGTCTGAAGTCAC<P7_index>ATCTCGTATGCCGTCTCTGCTTG --  
555     adapter2 AGATCGGAAGAGCGTCGTAGGGAAAGAGTGT<P5_index>  
556     GTGTAGATCTCGGTGGTCGCCGTATCATT --minlength <MIN_LEN>
```

557 With <P7_index> and <P5_index> defined by the i7/i5 index sequences for the given sample
558 and <MIN_LEN> set to 25 for charge tRNA-Seq using blunt-end ligation and 39 for charge tRNA-Seq
559 using splint assisted ligation. Each file with merged reads were then split based on adapter barcode.
560 A read was assigned to a particular adapter barcode if its 3' end had a substring within a hamming
561 distance of one to the barcode sequence, including the region complementary to the splint. The
562 adapter sequence was then trimmed off the 3' end; similarly, the 10 nt. UMI was located, saved
563 and trimmed off the 5' end, leaving only the tRNA sequence with possible 5' non-template bases
564 introduced during RT-PCR. Finally, samples with an excess of 2e6 reads were downsampled to 2e6
565 reads.

566 Trimmed reads were aligned to a masked reference as described below using the Smith-
567 Waterman algorithm implemented by SWIPE (*Rognes, 2011*):

```
568 swipe --symtype 1 --outfmt 7 --num_alignments 3 --num_descriptions 3 --evalue  
569     0.00000001 --strand 1 -G 6 -E 3 --matrix <SCORE_MATRIX>'
```

570 With an input score matrix (<SCORE_MATRIX>) defining a match score of 1, a mismatch score of -3
571 and a score for alignment to a masked reference position (N) of 0.

572 Alignment results were processed to extract three key data: 1) tRNA charge, 2) relative expression
573 level and 3) mismatches, gaps and RT truncations. First the alignment was parsed to extract
574 transcript annotation(s), alignment score and other relevant information. A read was assigned
575 the annotation with the highest alignment score and upon ties up to three annotations were
576 merged. When reporting data on the transcript level, a unique annotation was required for filtering,
577 when reporting at the codon level multiple annotations were allowed but a unique anticodon was
578 required and similarly for data on the amino acid level. Relative expression levels were calculated
579 as reads per million (RPM) with a count correction such that reads with identical sequence and
580 UMI were only counted once. Charge was calculated using uncorrected counts as this is a relative
581 number. Mismatches, gaps and RT truncations were extracted by redoing the Smith-Waterman
582 alignment between the read and its unmasked transcript annotation using a match score of 1, a
583 mismatch score of -2, a gap opening score of -3 and a gap extension score of -2. Using this new
584 alignment, mismatched, gaps and the index at the end of the alignment were extracted. Then
585 for each transcript the fraction of reads having mismatches and gaps at a given position was
586 calculated and the percentage drop in coverage at each position, referred to here as RT stops. For
587 both mutation, gap fractions and RT stops the UMI corrected read count was used. We provide a
588 boilerplate example of the whole read processing workflow on GitHub: https://github.com/krdav/tRNA-charge-seq/blob/main/projects/example/process_data.ipynb.

590 **Reference masking**

591 A human tRNA transcript reference for alignment was made from hg38 annotations in GtRNAdb
592 (*Chan and Lowe, 2016*). These sequences were deduplicated and mitochondrial tRNAs and spike-
593 in control sequences were appended. Then a BLAST database was generated, as required by
594 SWIPE, using the makeblastdb application. To further improve the alignment specificity, a masked
595 reference was made by converting positions with high likelihood of mismatch to Ns such that these
596 have no negative contribution on the alignment score. Position-wise mismatch frequency was
597 found as described above and filtered using a minimum of 200 transcript observations and 100
598 observations on each position. These were then turned into a masked reference using four tuning

parameters for picking the positions to mask. `unique_anno`: Only count reads with a unique transcript annotation. `min_mut_freq`: The minimum mismatch frequency to trigger masking. `frac_max_score`: The minimum fraction of the maximum alignment score between two reference sequences to expand the masked positions in one reference to another, requiring both positions to have the same nucleotide and the acceptor position to have less than 100 observations. The purpose is for an abundant transcript to donate its masking to a highly similar, but less abundant, transcript likely having the same RNA modifications. `iteration`: The number of masking iterations to perform. When changing the reference for alignment by masking the annotations can change, thus changing the position-wise mismatch frequency and the resulting reference masking. Running multiple iterations of reference masking stabilizes this change.

To find the optimal combination of tuning parameters a grid search was performed, testing all combinations of parameters shown in *Figure 3*, panel A. The objective of the search is to minimize the percentage of reads assigned to transcripts with multiple anticodons. Alternatively, the objective could be to minimize the percentage of reads assigned to multiple transcripts; however, this objective can lead the tuning parameters towards masking only a single transcript out of a family of highly similar transcripts, resulting in assignment of unique annotations to truncated reads, which cannot truly distinguish between transcripts of high similarity. This problem is less concerning using minimization of multiple anticodons since most families of highly similar transcripts have identical anticodons.

Barcode replicate test

For the barcode replicate test shown in *Figure 4*, the RNA used was first incubated 8 h at 20°C in intracellular physiological buffer, similar to the 8 h timepoint described in the aminoacylation half-life section below. This provided tRNA containing a spectrum of charge levels, spanning from almost fully acylated isoleucine tRNAs to almost fully deacylated asparagine tRNA. A single 10 µg sample of this RNA was then subjected to the one-pot Whitfeld reaction and subsequent tRNA isolation and ligation to each of the nine adapters as described for charge tRNA-Seq sample processing above.

Charge titration test

Whole cell RNA was reconstituted with 100 mM sodium acetate (pH=4.5) and adjusted to 1 µg/µL while keeping the RNA cold throughout. Half of this was moved to a fresh tube and deacylated by adding 5x volumes of 1 M lysine (pH=8), incubating at 45°C for 4 h and purifying using the Monarch RNA Cleanup Kit. Meanwhile, the other half was stored at -80°C. The concentration of the deacylated RNA was adjusted to 1 µg/µL and mixtures of intact and deacylated RNA was made using the following percentages of intact/deacylated RNA: 100/0, 85/15, 70/30, 55/45, 40/60, 25/75, 10/90, 0/100. Then these mixtures were subjected to the charge tRNA-Seq sample processing protocol described above with between 4 to 8 barcode replicates across independently prepared sequencing libraries, sequenced on different flow cells.

Reads were processed and the aminoacylation charge of each transcript was extracted to relate the measured with the predicted charge. However, the actual mixing ratios may deviate from the ones noted above due to inaccuracies in measuring the RNA concentration of intact and deacylated RNA, and due to depletion of certain tRNA species during the deacylation process, for example tRNAs sensitive to hydrolysis or depurination. We address this using a correction factor, F_i , described below. To calculate the predicted charge let A represent intact RNA, B represent deacylated RNA and the index i represent the transcript. Now, define the concentration, C , of a tRNA transcript i in the intact RNA as 1, while letting the concentration of the same tRNA transcript in the deacylated RNA be a fraction, F_i , of the intact RNA:

$$C_i^A = 1 \\ F_i = \frac{C_i^B}{C_i^A} \Leftrightarrow C_i^B = F_i \quad (2)$$

644 Then, define T_i^A as the measured charge of the intact tRNA of a transcript i averaged over the
645 replicates, and similarly T_i^B for deacylated RNA:

$$\begin{aligned} T_i^A &= \text{Avg charge}(A_i) \\ T_i^B &= \text{Avg charge}(B_i) \end{aligned} \quad (3)$$

646 Now, the predicted charge of a mixture of A and B can be defined using p to describe the percentage
647 of A in the mixture:

$$T_i^{AB}(p) = \frac{pT_i^A + (100 - p)T_i^B F_i}{p + (100 - p)F_i} \quad (4)$$

648 In the above, only F_i is unknown. The titration was made with 8 different mixing ratios, two of which
649 are used to calculating T_i^A and T_i^B , thus leaving 6 mixing ratios, each with several barcode replicates,
650 to fit F_i . Fitting was performed by minimizing the sum of squared differences between predicted
651 and measured charge using the Broyden–Fletcher–Goldfarb–Shanno (BFGS) algorithm with upper
652 and lower bound constraints of 4 and 0.25. Then **Equation 4** was used to calculate the predicted
653 charge and the difference to the measured charge was found and broken down by adapter barcode
654 to investigate ligation bias.

655 Aminoacetylation half-life

656 Whole cell RNA was reconstituted with 1 mM sodium acetate (pH=4.5) and adjusted to 1.5 µg/µL
657 while keeping the RNA cold throughout. A zero timepoint was then taken and 80 µL was transferred
658 to a PCR tube after which the experiment was started by adding 20 µL room temperature 5x
659 buffer, quickly mixing and placing the tube on a thermocycler set to 20°C. The buffer used was
660 an intracellular physiological buffer at 1x containing: 19 mM NaCl, 125 mM KCl, 0.33 mM CaCl₂,
661 1.4 mM MgCl₂, 0.5 mM spermidine, 30 mM HEPES, adjusted to pH=7.2 with KOH. Time from start
662 of incubation was tracked and samples drawn at the following timepoints: 4 min, 8 min, 16 min,
663 32 min, 1 h, 2 h, 4 h, 8 h, 16 h and 40 h. For the 40 h timepoint, two samples were drawn: one
664 standard and one receiving sham (NaCl) oxidation. Sample were taken by removing 8 µL, mixing it
665 in a prepared tube with 2 µL ice cold 500 mM sodium acetate (pH=4.5) and storing it at -80°C until
666 all timepoints were collected. This was repeated four times to generate independent replicates.
667 Then samples were processed similar to the charge tRNA-Seq protocol described above, but with
668 the three 5 min incubation times during periodate oxidation and quenching increased to 30 min
669 each due to the lower periodate solubility in the presence of potassium ions.

670 After read processing and alignment, data integrity was verified by checking that the E.coli tRNA
671 spike-in control and the non-oxidized 40 h samples conformed to expectations. RNA integrity at
672 the end of the experiment was also verified on a gel (**Figure 6—figure Supplement 1**, panel A). The
673 aminoacetylation charge was then calculated at the codon level and the data fitted to an equation
674 describing first-order decay:

$$N(t) = N_0 \left(\frac{1}{2} \right)^{\frac{t}{t_{1/2}}} + N_\infty \quad (5)$$

675 Where $N(t)$ is the charge of a given codon as a function of time, N_0 is the charge at time zero and
676 $t_{1/2}$ is the decay half-life. We added the N_∞ parameter to model the lower asymptote of charge to
677 accommodate the small fraction of tRNAs that still presents with a CCA-end after full deacylation.
678 The three parameters were fitted to the data by minimizing the sum of squared errors using the
679 Broyden–Fletcher–Goldfarb–Shanno (BFGS) algorithm with upper and lower bound constraints for
680 N_0 between 100 and 0 percent, for $t_{1/2}$ between 1e5 and 1 min and for N_∞ between 3.5 and 0 percent.
681 A point estimate for the three parameters were found using all timepoints and replicates and a
682 95% confidence interval was found using bootstrapping (N=1000) by sampling a single time-series
683 made up of random draws from the replicates (Supplementary file 4).

684 Data availability

685 Raw data and code for processing uploaded to: [some data dump link]
686 Python code available on Github: github.com/krdav/tRNA-charge-seq

687 Acknowledgments

688 We would like to acknowledge Arvind Rasi Subramaniam for suggesting we setup charge tRNA-Seq,
689 Alicia Darnell for sharing relevant samples and data and David Sokolov for help with early method
690 optimization.

691 Funding

692 L.B.S. acknowledges support from the National Institute of General Medical Sciences (NIGMS);
693 R35GM147118).

694 References

- 695 Alefelder S, Patel BK, Eckstein F. Incorporation of terminal phosphorothioates into oligonucleotides. Nucleic
696 Acids Res. 1998 Nov; 26(21):4983–4988.
- 697 Behrens A, Rodschinka G, Nedialkova DD. High-resolution quantitative profiling of tRNA abundance and
698 modification status in eukaryotes by mim-tRNAseq. Mol Cell. 2021 Feb; .
- 699 Chan PP, Lowe TM. GtRNADB 2.0: an expanded database of transfer RNA genes identified in complete and
700 draft genomes. Nucleic Acids Res. 2016 Jan; 44(D1):D184–9.
- 701 Clark WC, Evans ME, Dominissini D, Zheng G, Pan T. tRNA base methylation identification and quantification via
702 high-throughput sequencing. RNA. 2016 Nov; 22(11):1771–1784.
- 703 Cozen AE, Quartley E, Holmes AD, Hrabeta-Robinson E, Phizicky EM, Lowe TM. ARM-seq: AlkB-facilitated RNA
704 methylation sequencing reveals a complex landscape of modified tRNA fragments. Nat Methods. 2015 Sep;
705 12(9):879–884.
- 706 Dittmar KA, Sørensen MA, Elf J, Ehrenberg M, Pan T. Selective charging of tRNA isoacceptors induced by
707 amino-acid starvation. EMBO Rep. 2005 Feb; 6(2):151–157.
- 708 Dyer JR. Use of periodate oxidations in biochemical analysis. Methods Biochem Anal. 1956; 3:111–152.
- 709 Erber L, Hoffmann A, Fallmann J, Betat H, Stadler PF, Mörl M. LOTTE-seq (Long hairpin oligonucleotide based tRNA
710 high-throughput sequencing): specific selection of tRNAs with 3'-CCA end for high-throughput sequencing.
711 RNA Biol. 2020 Jan; 17(1):23–32.
- 712 Erskine JWB, Strouts CRN, Walley G, Lazarus W. A simple volumetric method for the routine determination of
713 glycerol. Analyst. 1953 Jan; 78(932):630–636.
- 714 Evans ME, Clark WC, Zheng G, Pan T. Determination of tRNA aminoacylation levels by high-throughput sequencing.
715 Nucleic Acids Res. 2017 Aug; 45(14):e133.
- 716 Fuchs RT, Sun Z, Zhuang F, Robb GB. Bias in ligation-based small RNA sequencing library construction is
717 determined by adaptor and RNA structure. PLoS One. 2015 May; 10(5):e0126049.
- 718 Heinemann IU, Nakamura A, O'Donoghue P, Eiler D, Söll D. tRNAHis-guanylyltransferase establishes tRNAHis
719 identity. Nucleic Acids Res. 2012 Jan; 40(1):333–344.
- 720 Hentzen D, Mandel P, Garel JP. Relation between aminoacyl-tRNA stability and the fixed amino acid. Biochim
721 Biophys Acta. 1972 Oct; 281(2):228–232.
- 722 Hernandez-Alias X, Katanski CD, Zhang W, Assari M, Watkins CP, Schaefer MH, Serrano L, Pan T. Single-read
723 tRNA-seq analysis reveals coordination of tRNA modification and aminoacylation and fragmentation. Nucleic
724 Acids Res. 2022 Dec; .
- 725 Ho YS, Kan YW. In vivo aminoacylation of human and Xenopus suppressor tRNAs constructed by site-specific
726 mutagenesis. Proc Natl Acad Sci U S A. 1987 Apr; 84(8):2185–2188.
- 727 Hoffmann A, Fallmann J, Vilardo E, Mörl M, Stadler PF, Amman F. Accurate mapping of tRNA reads. Bioinformatics.
728 2018 Apr; 34(7):1116–1124.
- 729 Holcomb CL, Rastrou M, Williams TC, Goodridge D, Lazaro AM, Tilanus M, Erlich HA. Next-generation sequencing
730 can reveal in vitro-generated PCR crossover products: some artifactual sequences correspond to HLA alleles
731 in the IMGT/HLA database. Tissue Antigens. 2014 Jan; 83(1):32–40.

- 732 **Jayaprakash AD**, Jabado O, Brown BD, Sachidanandam R. Identification and remediation of biases in the activity
733 of RNA ligases in small-RNA deep sequencing. *Nucleic Acids Res.* 2011 Nov; 39(21):e141.
- 734 **Katanski CD**, Watkins CP, Zhang W, Reyer M, Miller S, Pan T. Analysis of queuosine and 2-thio tRNA modifications
735 by high throughput sequencing. *Nucleic Acids Res.* 2022 Sep; 50(17):e99.
- 736 **Khym JX**, Cohn WE. Amine-induced cleavage of periodate-oxidized nucleotide residues. *J Biol Chem.* 1961 Mar;
737 236:PC9–10.
- 738 **Khym JX**, Uziel M. The use of the cetyltrimethylammonium cation in terminal sequence analyses of ribonucleic
739 acids. *Biochemistry.* 1968 Jan; 7(1):422–426.
- 740 **Kroll H**. The Participation of Heavy Metal Ions in the Hydrolysis of Amino Acid Esters1. *J Am Chem Soc.* 1952
741 Apr; 74(8):2036–2039.
- 742 **Langmead B**, Salzberg SL. Fast gapped-read alignment with Bowtie 2. *Nat Methods.* 2012 Mar; 9(4):357–359.
- 743 **Langmead B**, Trapnell C, Pop M, Salzberg SL. Ultrafast and memory-efficient alignment of short DNA sequences
744 to the human genome. *Genome Biol.* 2009 Mar; 10(3):R25.
- 745 **Lentini JM**, Ramos J, Fu D. Monitoring the 5-methoxycarbonylmethyl-2-thiouridine (mcm5s2U) modification in
746 eukaryotic tRNAs via the γ -toxin endonuclease. *RNA.* 2018 May; 24(5):749–758.
- 747 **Lucas MC**, Pryszcz LP, Medina R, Milenkovic I, Camacho N, Marchand V, Motorin Y, Ribas de Pouplana L, Novoa
748 EM. Quantitative analysis of tRNA abundance and modifications by nanopore RNA sequencing. *Nat Biotechnol.*
749 2023 Apr; p. 1–15.
- 750 **McGlinny NJ**, Ingolia NT. Transcriptome-wide measurement of translation by ribosome profiling. *Methods.*
751 2017 Aug; 126:112–129.
- 752 **Mohr S**, Ghanem E, Smith W, Sheeter D, Qin Y, King O, Polioudakis D, Iyer VR, Hunicke-Smith S, Swamy S, Kuersten
753 S, Lambowitz AM. Thermostable group II intron reverse transcriptase fusion proteins and their use in cDNA
754 synthesis and next-generation RNA sequencing. *RNA.* 2013 Jul; 19(7):958–970.
- 755 **Motorin Y**, Muller S, Behm-Ansmant I, Branlant C. Identification of Modified Residues in RNAs by Reverse
756 Transcription-Based Methods. In: *Methods in Enzymology*, vol. 425 Academic Press; 2007.p. 21–53.
- 757 **Neu HC**, Heppel LA. NUCLEOTIDE SEQUENCE ANALYSIS OF POLYRIBONUCLEOTIDES BY MEANS OF PERIODATE
758 OXIDATION FOLLOWED BY CLEAVAGE WITH AN AMINE. *J Biol Chem.* 1964 Sep; 239:2927–2934.
- 759 **Pavlova NN**, King B, Josselsohn RH, Violante S, Macera VL, Vardhana SA, Cross JR, Thompson CB. Translation in
760 amino-acid-poor environments is limited by tRNAGln charging. *Elife.* 2020 Dec; 9.
- 761 **Peacock JR**, Walvoord RR, Chang AY, Kozlowski MC, Gamper H, Hou YM. Amino acid-dependent stability of the
762 acyl linkage in aminoacyl-tRNA. *RNA.* 2014 Jun; 20(6):758–764.
- 763 **Pinkard O**, McFarland S, Sweet T, Coller J. Quantitative tRNA-sequencing uncovers metazoan tissue-specific
764 tRNA regulation. *Nat Commun.* 2020 Aug; 11(1):4104.
- 765 **Rammler DH**. Periodate oxidations of enamines. I. Oxidation of adenosine 5'-monophosphate in the presence
766 of methylamine. *Biochemistry.* 1971 Dec; 10(25):4699–4705.
- 767 **Rao YS**, Cherayil JD. Studies on chemical modification of thionucleosides in the transfer ribonucleic acid of
768 *Escherichia coli*. *Biochem J.* 1974 Nov; 143(2):285–294.
- 769 **Rognes T**. Faster Smith-Waterman database searches with inter-sequence SIMD parallelisation. *BMC Bioinformatics.*
770 2011 Jun; 12:221.
- 771 **Saraiva MA**, Borges CM, Florêncio MH. Reactions of a modified lysine with aldehydic and diketonic dicar-
772 bonyl compounds: an electrospray mass spectrometry structure/activity study. *J Mass Spectrom.* 2006 Feb;
773 41(2):216–228.
- 774 **Sas-Chen A**, Schwartz S. Misincorporation signatures for detecting modifications in mRNA: Not as simple as it
775 sounds. *Methods.* 2019 Mar; 156:53–59.
- 776 **Schofield P**, Zamecnik PC. Cupric ion catalysis in hydrolysis of aminoacyl-tRNA. *Biochim Biophys Acta.* 1968
777 Feb; 155(2):410–416.

- 778 **Shigematsu M**, Honda S, Loher P, Telonis AG, Rigoutsos I, Kirino Y. YAMAT-seq: an efficient method for
779 high-throughput sequencing of mature transfer RNAs. *Nucleic Acids Res.* 2017 May; 45(9):e70.
- 780 **Smith AM**, Abu-Shumays R, Akeson M, Bernick DL. Capture, Unfolding, and Detection of Individual tRNA
781 Molecules Using a Nanopore Device. *Front Bioeng Biotechnol.* 2015 Jun; 3:91.
- 782 **Stenum TS**, Sørensen MA, Svenningsen SL. Quantification of the Abundance and Charging Levels of Transfer
783 RNAs in *Escherichia coli*. *J Vis Exp.* 2017 Aug; 1(126).
- 784 **Thomas NK**, Poodari VC, Jain M, Olsen HE, Akeson M, Abu-Shumays RL. Direct Nanopore Sequencing of Individual
785 Full Length tRNA Strands. *ACS Nano.* 2021 Oct; 15(10):16642–16653.
- 786 **Tsukamoto Y**, Nakamura Y, Hirata M, Sakate R, Kimura T. i-tRAP (individual tRNA acylation PCR): A convenient
787 method for selective quantification of tRNA charging. *RNA.* 2022 Oct; 29(1):111–122.
- 788 **Uziel M**. Amine-catalyzed elimination of beta-phosphoric esters from aldehydes derived from ribonucleic acid
789 and model substrates. *Arch Biochem Biophys.* 1975 Jan; 166(1):201–212.
- 790 **Uziel M**. Periodate oxidation and amine-catalyzed elimination of the terminal nucleoside from adenylate or
791 ribonucleic acid. Products of overoxidation. *Biochemistry.* 1973; 12(5):938–942.
- 792 **Varshney U**, Lee CP, RajBhandary UL. Direct analysis of aminoacylation levels of tRNAs in vivo. Application to
793 studying recognition of *Escherichia coli* initiator tRNA mutants by glutamyl-tRNA synthetase. *J Biol Chem.*
794 1991 Dec; 266(36):24712–24718.
- 795 **Wang J**, Toffano-Nioche C, Lorieux F, Gautheret D, Lehmann J. Accurate characterization of *Escherichia coli* tRNA
796 modifications with a simple method of deep-sequencing library preparation. *RNA Biol.* 2021 Jan; 18(1):33–46.
- 797 **Warren JM**, Salinas-Giegé T, Hummel G, Coots NL, Svendsen JM, Brown KC, Drouard L, Sloan DB. Combining
798 tRNA sequencing methods to characterize plant tRNA expression and post-transcriptional modification. *RNA Biol.*
799 2021 Jan; 18(1):64–78.
- 800 **Watkins CP**, Zhang W, Wylder AC, Katanski CD, Pan T. A multiplex platform for small RNA sequencing elucidates
801 multifaceted tRNA stress response and translational regulation. *Nat Commun.* 2022 May; 13(1):2491.
- 802 **Whitfeld PR**. A method for the determination of nucleotide sequence in polyribonucleotides. *Biochem J.* 1954
803 Nov; 58(3):390–396.
- 804 **Whitfeld PR**, Markham R. Natural configuration of the purine nucleotides in ribonucleic acids; chemical
805 hydrolysis of the dinucleoside phosphates. *Nature.* 1953 Jun; 171(4365):1151–1152.
- 806 **Wolfson AD**, Uhlenbeck OC. Modulation of tRNA^{Ala} identity by inorganic pyrophosphatase. *Proc Natl Acad Sci
807 U S A.* 2002 Apr; 99(9):5965–5970.
- 808 **Yamagami R**, Hori H. Application of mutational profiling: New functional analyses reveal the tRNA recognition
809 mechanism of tRNA m1A22 methyltransferase. *J Biol Chem.* 2022 Dec; 299(1):102759.
- 810 **Zheng G**, Qin Y, Clark WC, Dai Q, Yi C, He C, Lambowitz AM, Pan T. Efficient and quantitative high-throughput
811 tRNA sequencing. *Nat Methods.* 2015 Sep; 12(9):835–837.
- 812 **Zhuang F**, Fuchs RT, Sun Z, Zheng Y, Robb GB. Structural bias in T4 RNA ligase-mediated 3'-adapter ligation.
813 *Nucleic Acids Res.* 2012 Apr; 40(7):e54.
- 814 **Ziff EB**, Fresco JR. Chemical transformation of 4-thiouracil nucleosides to uracil and cytosine counterparts. *J Am
815 Chem Soc.* 1968 Dec; 90(26):7338–7342.

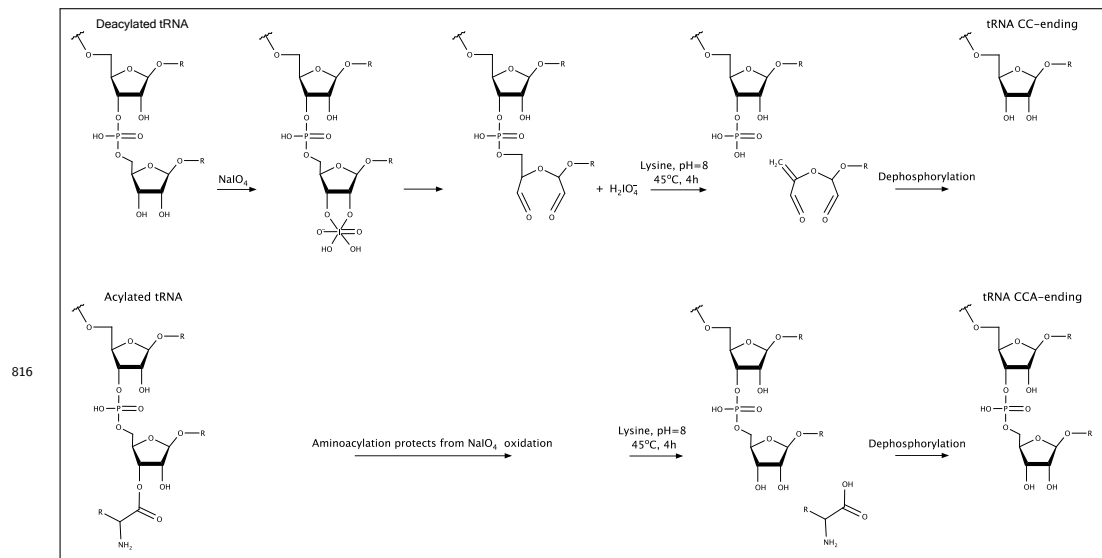


Figure 1—figure supplement 1. Schematic of the Whitfeld reaction with acylated and deacylated tRNA leading to generation of CCA and CC-ending tRNAs. For deacylated tRNA, 3' adenose is oxidized by periodate and then cleaved off by lysine induced β -elimination (**Rammel, 1971; Uziel, 1973**). Acylated tRNA is protected from periodate oxidation but will be deacylated in the subsequent incubation with lysine.

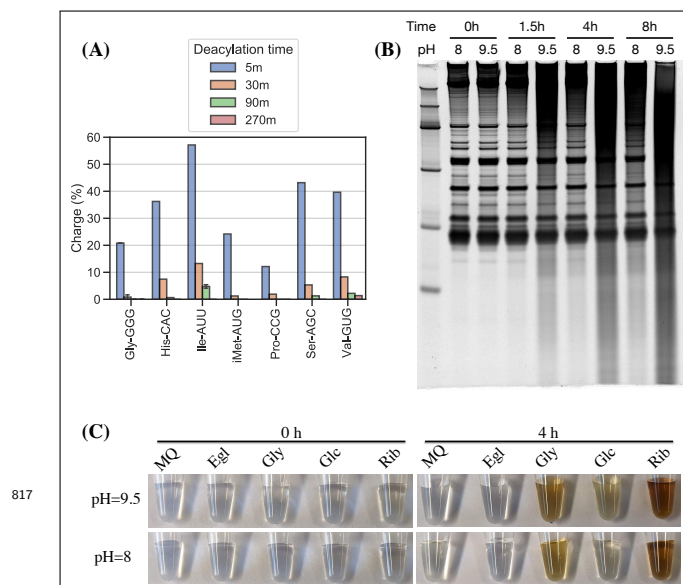


Figure 2—figure supplement 1. Optimizing lysine induced cleavage for the charge tRNA-Seq method. **(A)** Aminoacylation remaining after 5, 30, 90 and 270 min of deacylation in 1 M lysine pH=8 at 45°C. After deacylation, RNA was purified and submitted to the Whitfeld reaction using lysine cleavage at pH=9.5 for 90 min at 45°C to ensure complete deacylation. The RNA was then processed using the described charge tRNA-Seq method. **(B)** RNA stability over time for lysine cleavage at pH=8 and borax cleavage at pH=9.5. **(C)** Lysine reacts with dialdehydes forming from quencher oxidation. One-pot Whitfeld reactions were performed at pH=8 and pH=9.5 and quenched with either water (MQ), ethylene glycol (Egl), glycerol (Gly), glucose (Glc) or ribose (Rib). Pictures taken before (0 h) and after (4 h) the lysine cleavage step indicate side product formation consistent with lysine reacting with dialdehydes formed during the periodate quenching (**Saraiva et al., 2006**). This side product causes problems in the later purification step.

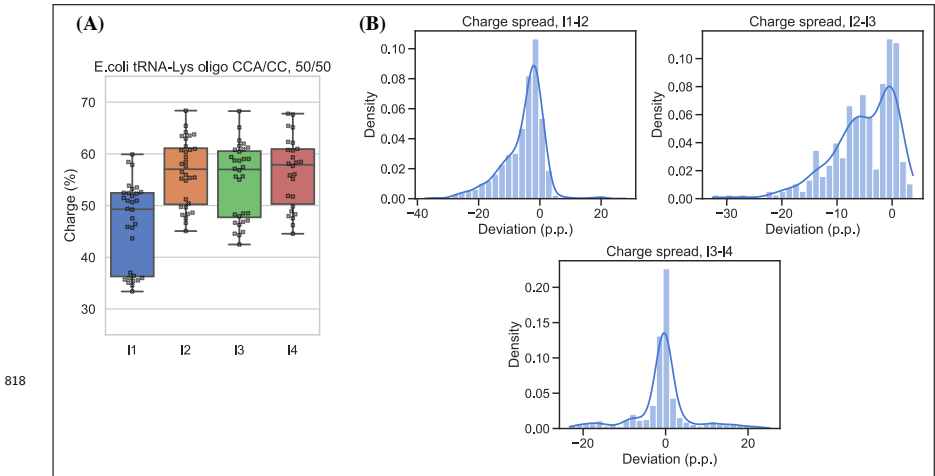


Figure 2—figure supplement 2. Measurement bias in charge tRNA-Seq using blunt-end ligation. **(A)** Measured charge of a E.coli tRNA-Lys oligo control spiked into samples processed with four different pre-adenylated adapters using the method described by *Behrens et al. (2021)*. The control was made using a mix of 50% E.coli tRNA-Lys-CCA and 50% E.coli tRNA-Lys-CC and thus simulating 50% charge. Each dot represents a single charge tRNA-Seq sample. **(B)** Distribution of charge differences at the transcript level among samples with two barcode replicates, comparing adapters I1 vs. I2, I2 vs. I3 and I3 vs. I4. Deviation is reported as percentage point differences and the kernel density estimate (KDE) is overlaid.

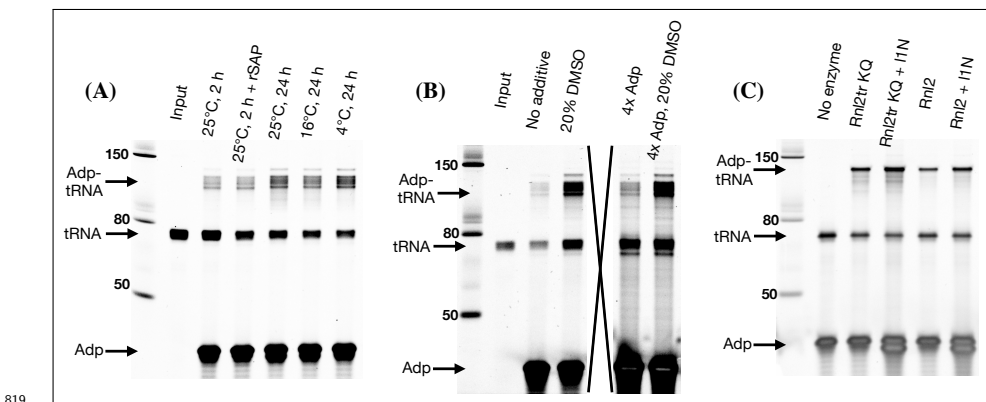


Figure 2—figure supplement 3. Despite optimization attempts, high ligation efficiency could not be achieved for blunt-end ligation. **(A)** Effect of incubation temperature, time and addition of a phosphatase (rSAP). Using deacylated and gel purified human tRNA as substrate and pre-adenylated I3N as adapter, otherwise following the method in *Behrens et al. (2021)*. **(B)** Effect of additives and higher adapter concentration. Using deacylated and gel purified human tRNA as substrate, pre-adenylated I2N as adapter and 4°C, 24 h incubation. An irrelevant well has been crossed out to avoid image splicing. **(C)** Effect of ligase type. Using the E.coli tRNA-Lys-CCA oligo as substrate, pre-adenylated I1N as adapter and 4°C, 24 h incubation with 20% DMSO. Wells with "+I1N" were added additional none pre-adenylated adapter. RnL2tr KQ (T4 RNA Ligase 2, truncated KQ) is the standard ligase used for pre-adenylated adapters whereas RnL2 (T4 RNA Ligase 2) does not require pre-adenylation of adapters.

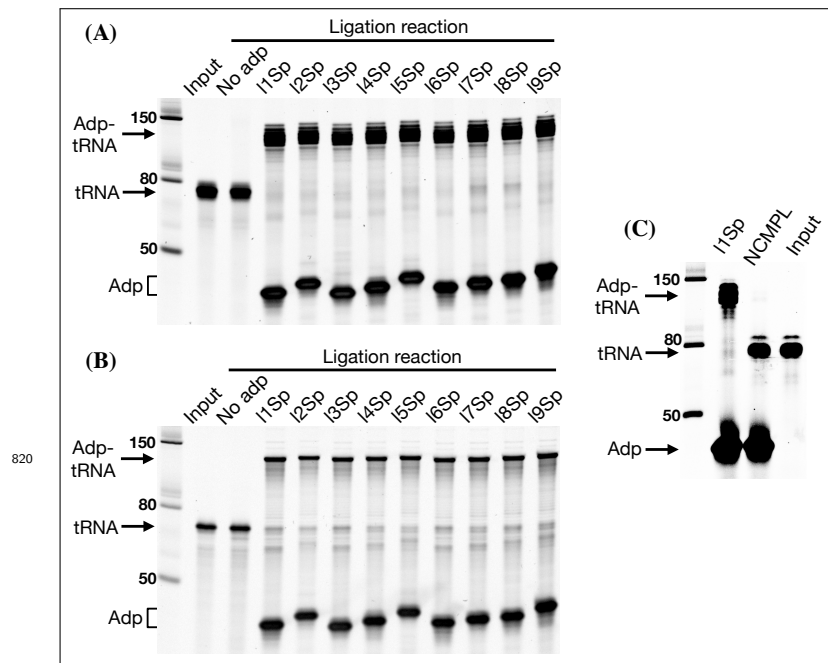


Figure 2—figure supplement 4. Ligation efficiency of all the barcoded adapters is high and depends on splint complementarity. **(A)** Ligation reactions using deacylated purified human tRNA as substrate. **(B)** Ligation reactions using E.coli tRNA-Lys-CC oligo as substrate. **(C)** Comparing ligation using a tRNA-end complementary splint (l1Sp lane) vs. a non-complementary splint (NCMPL lane). For both ligations the l1Sp adapter was used. For the non-complementary splint ligation the two standard TGGN and GGN overhang generating splints were swapped by two splints generating CAAC and AAC overhangs.

820

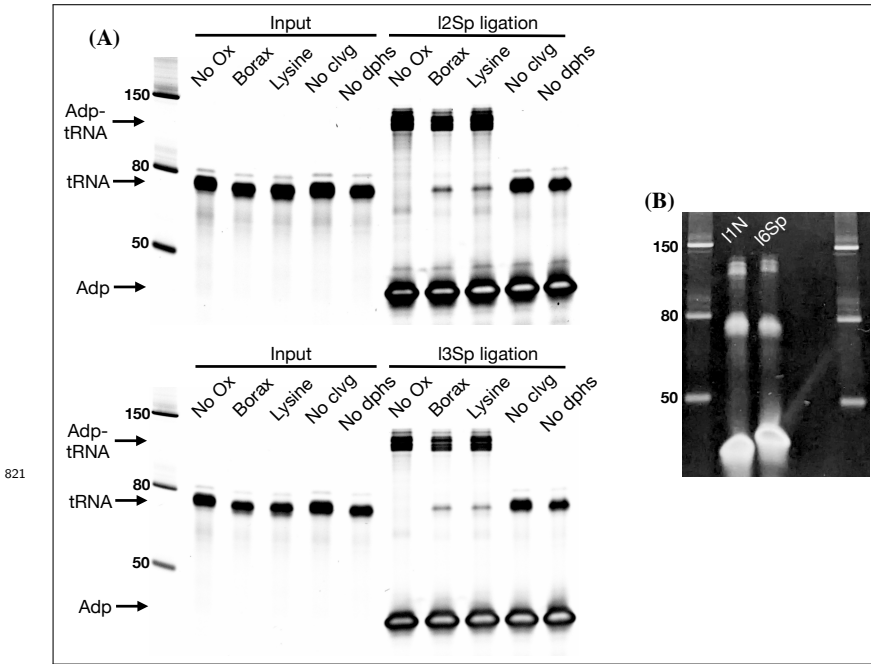


Figure 2—figure supplement 5. (A) Ligation test comparing the effect of RNA processing. Similar to **Figure 2**, panel E but with two different adapters. **(B)** The unligated tRNA that appears after tRNA is oxidized with periodate in panel A is refractory to further ligation. The unligated tRNA was gel purified from enough ligation reactions as shown in panel A to setup two new ligation reactions using either I₁N pre-adenylated adapter for blunt end ligation or I₆SP for splint assisted ligation. For I₁N, ligation was setup with 35 ng tRNA, 20 pmol adapter, 17.5% PEG-8000, 20% DMSO, 1xT4 RNA ligase buffer, 1 μ L T4 RNA ligase 2 (truncated KQ) and 1 μ L Superaseln. For I₆SP, the ligation was setup as described in the charge tRNA-Seq protocol.

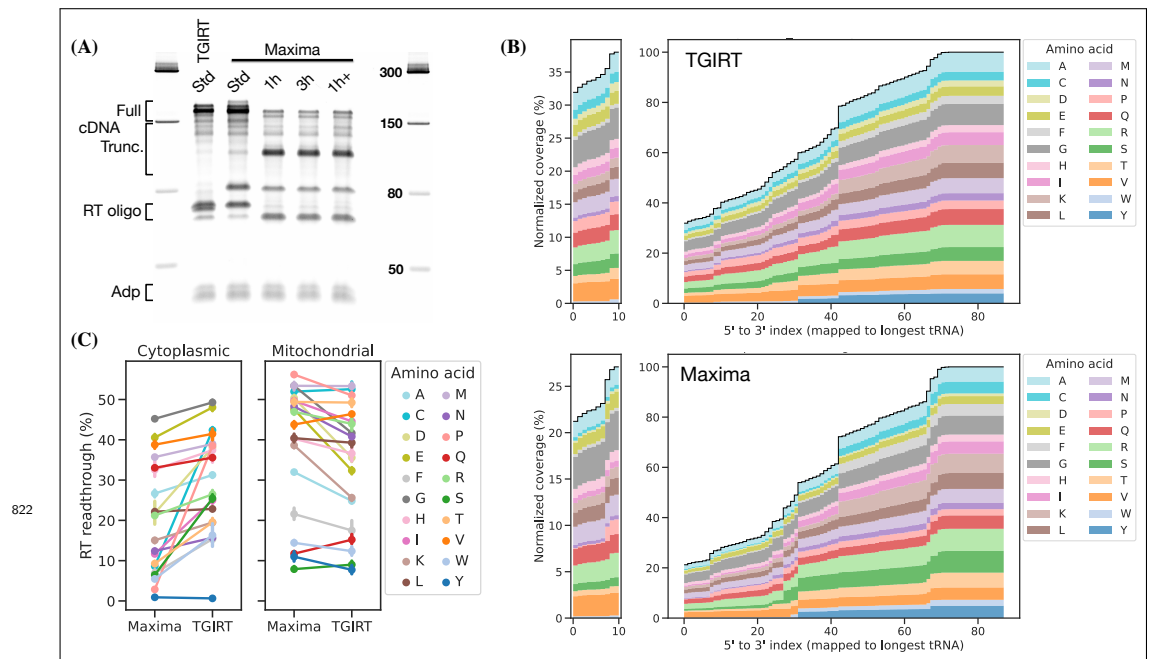


Figure 2—figure supplement 6. (A) The Maxima RT polymerase produces similar levels of full size cDNA as TGIRT-III under the standard (Std) tRNA-Seq RT-PCR conditions (42°C , 16 h, suggested by [Behrens et al. \(2021\)](#)). For Maxima, other incubation conditions tested are: 1 h at 60°C (similar to [Lucas et al. \(2023\)](#)), 3 h at 60°C and 1 h at 60°C followed by 15 h at 42°C (1h+). After RT-PCR, the RNA template was removed by NaOH hydrolysis, liberating the DNA adapter annotated on the gel. **(B)** Coverage plots for cytoplasmic tRNA transcripts grouped by cognate amino acid, comparing samples prepared with TGIRT-III or Maxima using standard incubation (42°C , 16 h). **(C)** Percentage of full length transcripts grouped by cognate amino acid (i.e. left side of plots in panel B). Errorbars are bootstrapped 95% confidence interval of the mean over the 7 individual samples barcoded, pooled and used for RT-PCR template with both TGIRT-III and Maxima.

822

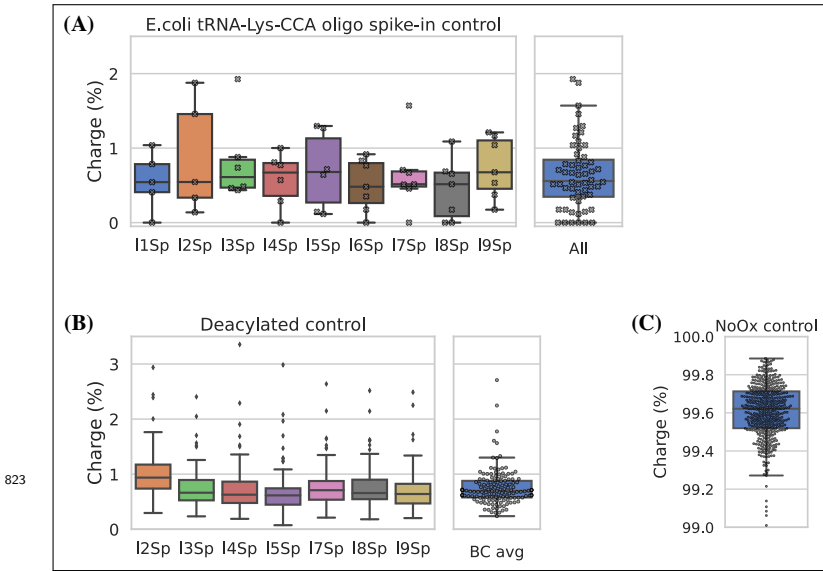


Figure 2—figure supplement 7. Charge tRNA-Seq control samples and spike-ins validate the method. **(A)** Cleavage of the 3' adenosine on spike-in oligo is near complete and similarly measured across adapters. Using the E.coli tRNA-Lys-CCA oligo as a spike-in control to monitor completion of the Whitfeld reaction. If complete, 100% E.coli tRNA-Lys-CC should be produced and thus appearing as 0% charged. Each dot represents one sample spiked with E.coli tRNA-Lys-CCA oligo before the Whitfeld reaction and processed using the charge tRNA-Seq processing described in the method section. **(B)** Aminoacylation level of human tRNA transcripts after undergoing deacylation by incubation at 45°C for 4 h in 1 M lysine (pH=8). Mitochondrial tRNA^{fMet} was excluded because formylated amino acids are known to be highly resistant towards deacylation (*Schofield and Zamecnik, 1968*). **(C)** Aminoacylation level of tRNA transcripts from four samples receiving sham oxidation (NaCl) during the Whitfeld reaction.

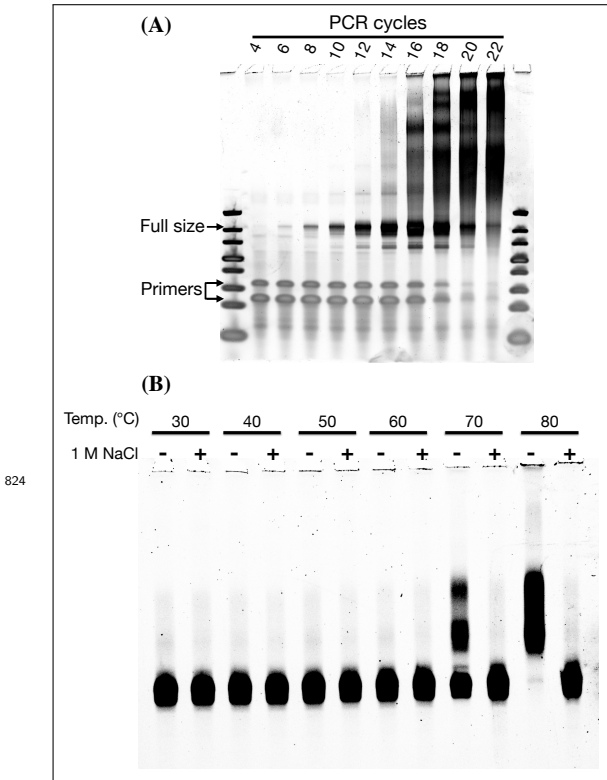


Figure 2—figure supplement 8. **(A)** The specificity of the final library PCR step (attaching Illumina P7 and P5 sequences) deteriorates with increasing product-to-primer ratios, probably due to high tRNA homology and PCR crossover (*Holcomb et al., 2014*). **(B)** tRNA-Seq DNA library reannealing is inhibited by high salt concentrations. A gel purified charge tRNA-Seq DNA library was resuspended in TBE buffer and incubated 30 min at different temperatures with or without 1 M NaCl.

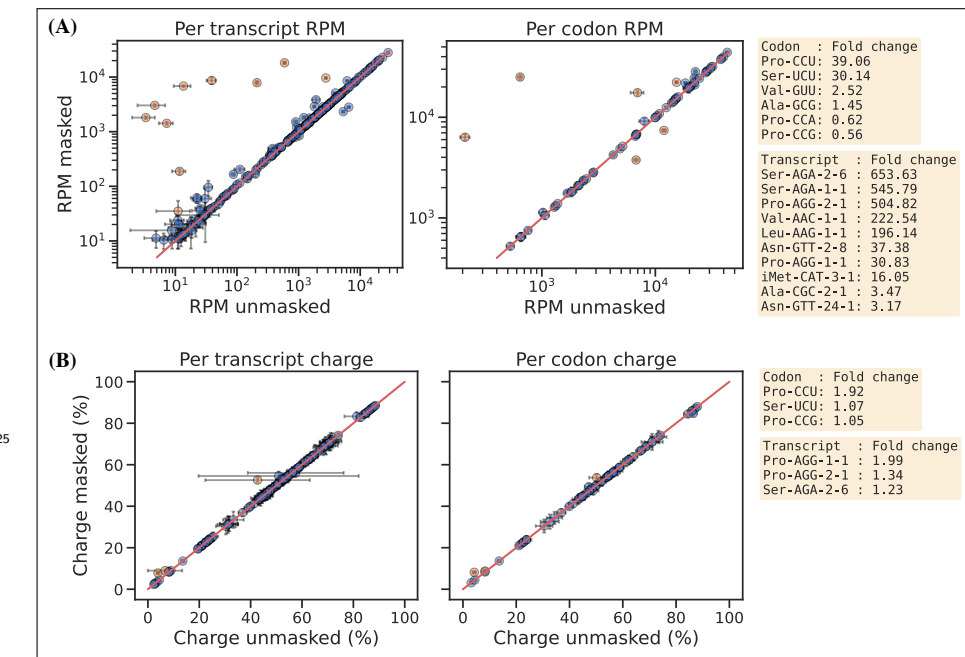


Figure 3—figure supplement 1. **(A)** Reference masking effect on RPM levels per transcript (left) and per codon (right). Transcripts showing > 3, and codons showing > 1.4, fold increase or decrease upon reference masking are colored orange and annotated on the right side of the plot. **(B)** Reference masking effect on charge levels per transcript (left) and per codon (right). Transcripts/codons showing > 1.05 fold increase or decrease upon reference masking are colored orange and annotated on the right side of the plot.

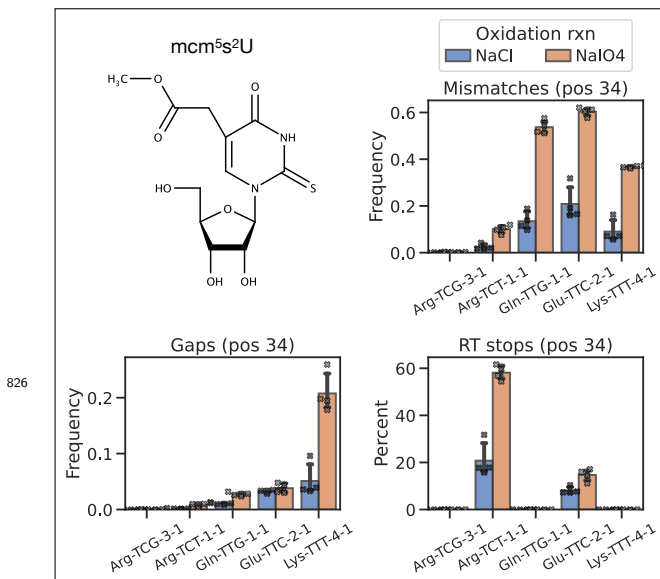


Figure 3—figure supplement 2. Mismatch frequency, gap frequency and RT stop percentage is increased upon periodate oxidation for transcripts known to be 5-methoxycarbonylmethyl-2-thiouridine (mcm5s2U) modified. The mcm5s2U modification has been shown to be present on the first anticodon nucleoside (position 34) in human tRNA Lys-UUU, Gln-UUG, Glu-UUC and Arg-UCU, while absent in the similar tRNA Arg-UCG (*Lentini et al., 2018*).

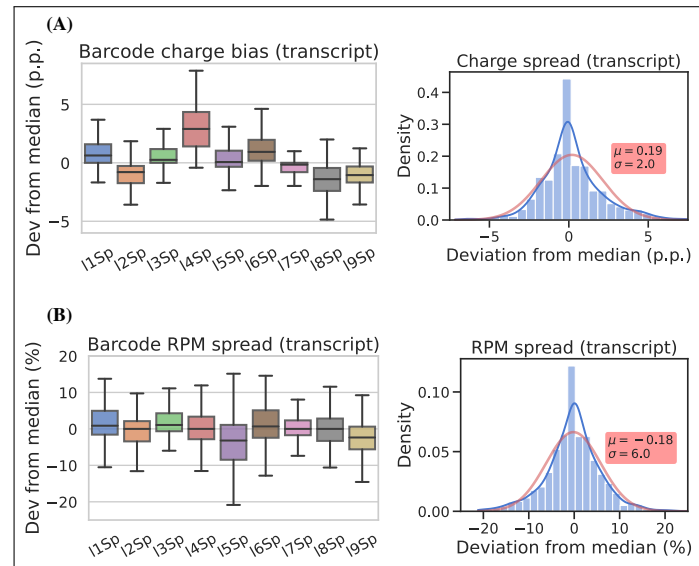


Figure 4—figure supplement 1. Similar to **Figure 4**, but at the transcript level.

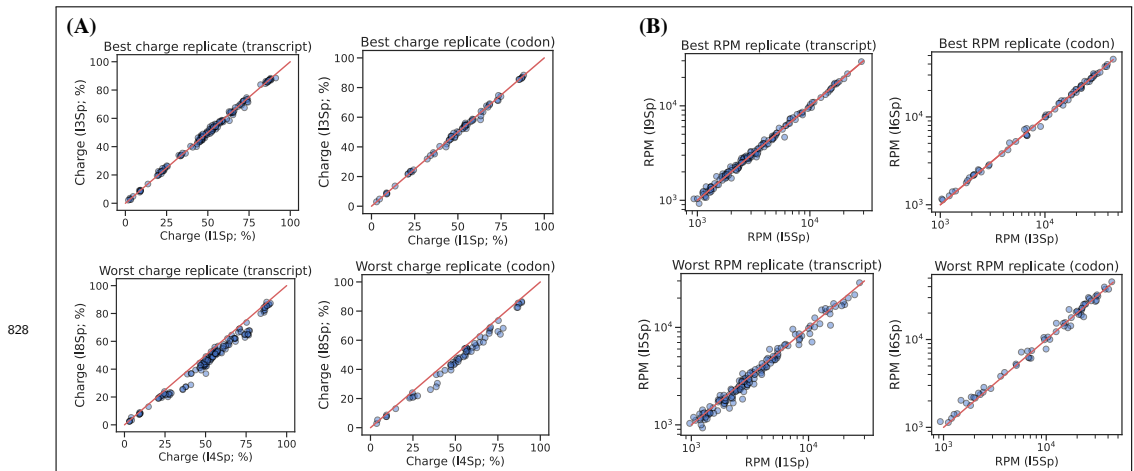


Figure 4—figure supplement 2. Best and worst pairwise comparisons between barcode replicates. Sorting pairwise comparisons between barcode replicates according to the sum of squared differences and showing the best and worst either at the transcript or codon level. **(A)** For charge levels, adapter I4Sp tends to overestimate charge. **(B)** For RPM levels. For all plots the red line is proportionality.

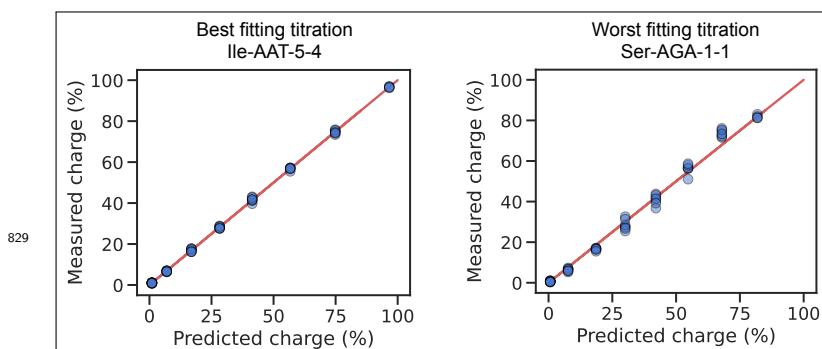


Figure 5—figure supplement 1. The best and worst transcript when ranked based on the sum of squared differences between the measured and predicted charge. Related to the representative (i.e. ranked as the median) transcript shown in **Figure 5**, panel B.

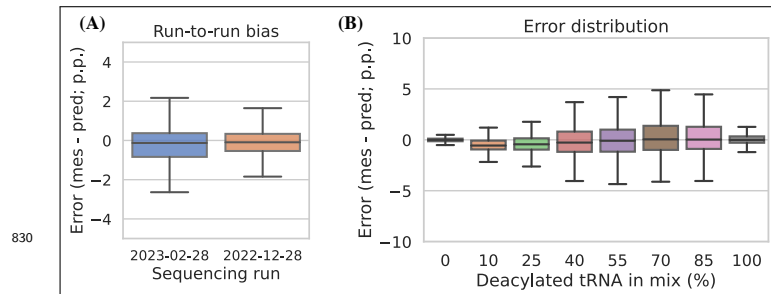


Figure 5—figure supplement 2. Charge titration prediction error binned by sequencing run and titration sample. **(A)** Run-to-run bias of two sequencing libraries independently prepared and sequenced on different days. **(B)** Error distribution binned by titration sample. In both panels, error is the percentage point difference between the measured vs. predicted charge for all transcripts in the bin.

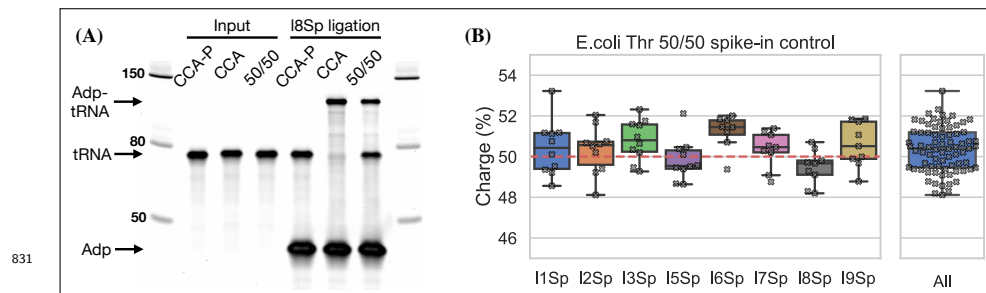


Figure 5—figure supplement 3. Spike-in control for 50% charge using the E.coli tRNA-Thr-CGT oligo. **(A)** Ligation between E.coli tRNA-Thr-CCA-Phos and I8Sp is completely blocked indicating ~100% 3' phosphorylation. CCA-P, E.coli tRNA-Thr-CCA-Phos. CCA, E.coli tRNA-Thr-CCA. 50/50, equal mix of CCA-p and CCA. **(B)** E.coli tRNA-Thr spike-in charge measured for samples prepared with an equimolar mix of E.coli tRNA-Thr-CCA-Phos and E.coli tRNA-Thr-CCA. Each dot represents a single charge tRNA-Seq sample. The red dashed line indicates 50% charge.

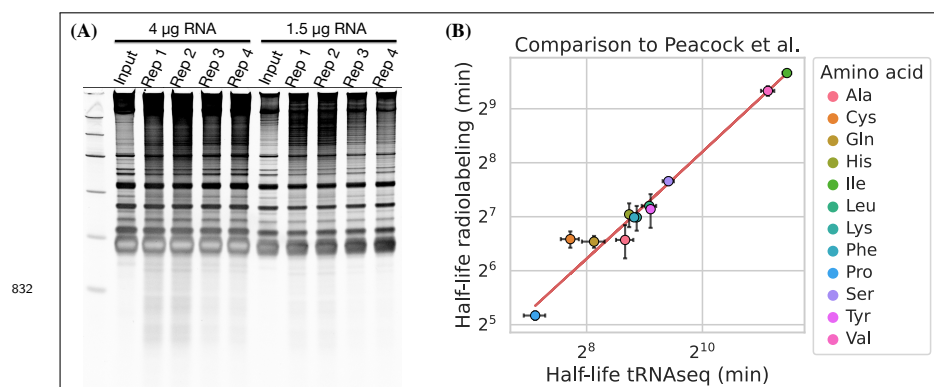


Figure 6—figure supplement 1. **(A)** RNA integrity after the last sample was taken (40 h) for the four replicates in the aminoacylation half-life experiment. **(B)** Comparison between aminoacylation half-life estimates grouped by amino acid from this study (tRNaseq) and measurements by *Peacock et al. (2014)* (radiolabeling). Errorbars are +/- standard deviations. A linear regression line is shown as a red line.

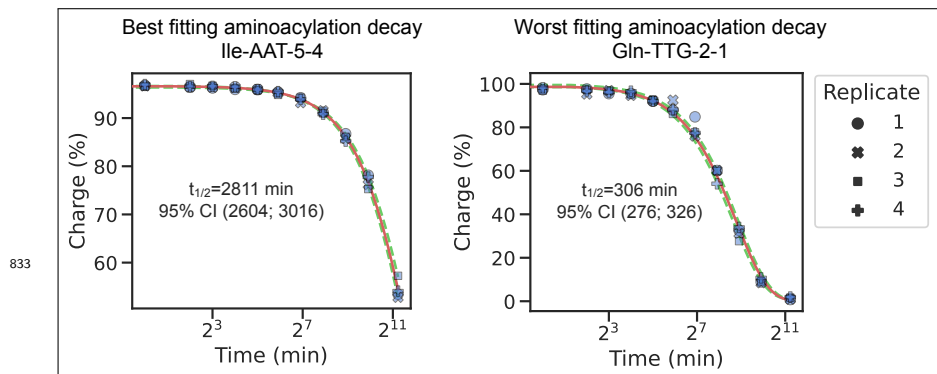


Figure 6—figure supplement 2. The best and worst transcript half-life estimates, ranked based on the sum of squared differences between the fitted decay function and the mean charge of the replicates. Related to the representative (i.e. ranked as the median) transcript shown in *Figure 6*, panel A.